2016

# Long-term monitoring of biophysical characteristics of tidal wetlands in the northern Gulf of Mexico — A methodological approach using MODIS

Shuvo Ghosh
*UGA*, shubho@uga.edu

Deepak Mishra
*UGA*, dmishra@uga.edu

Remote Sensing of Environment 173 (2016) 39–58

Contents lists available at ScienceDirect

Remote Sensing of Environment

journal homepage: www.elsevier.com/locate/rse

# Long-term monitoring of biophysical characteristics of tidal wetlands in the northern Gulf of Mexico — A methodological approach using MODIS

Shuvankar Ghosh [a,*], Deepak R. Mishra [a,*], Anatoly A. Gitelson [b,c]

[a] Center for Geospatial Research, Department of Geography, University of Georgia, 210 Field Street, Rm. 204, Athens, GA 30605, USA
[b] School of Natural Resources, University of Nebraska–Lincoln, USA
[c] Department of Civil and Environmental Engineering, Israel Institute of Technology, Technion City, Haifa, Israel

ARTICLE INFO

*Article history:*
Received 27 February 2015
Received in revised form 10 November 2015
Accepted 13 November 2015
Available online 5 December 2015

*Keywords:*
Gulf of Mexico
Tidal wetlands
Remote sensing
Biophysical characteristics
Green leaf area index
Green vegetation fraction
Canopy chlorophyll
Above ground biomass
Field spectroscopy
MODIS

ABSTRACT

Accurate and efficient monitoring is critically important for the effective restoration and conservation of threatened tidal wetlands in the Gulf Coast. The high carbon sequestration potential, habitat for important wildlife and fish, and numerous ecosystem services make these tidal wetlands highly valuable both ecologically and economically to Gulf Coast communities. Our study developed a new methodological approach for mapping biophysical health of coastal tidal wetland habitats in terms of green leaf area index (GLAI), canopy level chlorophyll content (CHL), vegetation fraction (VF), and above ground green biomass (GBM). We measured these biophysical characteristics in tidal wetlands of the northern Gulf of Mexico using a combination of ground data collected from field surveys during the growing seasons of 2010 and 2011 and NASA's Moderate Resolution Imaging Spectroradiometer (MODIS) 250 m and 500 m images. Additionally, we compared and evaluated the performances of both *in situ* proximal and satellite remote sensing measurements in terms of their potential for mapping the wetland biophysical characteristics. MODIS-based models proved superior at the landscape level compared to models developed from *in situ* proximal sensing, as species level signals seemed to be diluted at coarser spatial scales. We selected Wide Dynamic Range Vegetation Index (WDRVI) for MODIS 250 m and Visible Atmospheric Resistant Index (VARI) for MODIS 500 m to map biophysical characteristics of tidal wetlands. Time-series composites and phenological information derived using the MODIS based models captured the impact of the selected disturbances in the last decade on the ecological and physiological status of the tidal wetland habitats in the Gulf Coast. This is the first study to employ MODIS data to analyze the biophysical characteristics of tidal wetlands in the Gulf Coast, which, in turn, has the potential to improve our ability to predict their productivity and carbon sequestration potential. These techniques could also be used to assess the success of previous and ongoing tidal wetland restoration projects, and evaluate the productivity of marshes under threat from developmental activity, sea level rise, and industrial pollution.



## 1. Introduction

Tidal wetlands are one of the most ecologically and economically productive and vulnerable ecosystems in the world (Mitsch & Gosselink, 2007; Tiner, 2013). Thriving at the confluence of marine and terrestrial systems, they serve as critical habitats for fish and wildlife, as well as species, which are commercially valuable to the local community. These ecosystems also help buffer and maintain shorelines, clean natural waters, reduce siltation in navigable waters, and potentially help in storing floodwaters (Barbier et al., 2008; Boesch & Turner, 1984; Deegan, Hughes, & Rountree, 2002; Koch et al., 2009; Morgan, Burdick, & Short, 2009). Furthermore, in light of exponential increases in atmospheric $CO_2$ in recent decades, the high Carbon Sequestration Potential (CSP) of tidal wetlands makes them critical carbon sinks for atmospheric greenhouse gases (Brevik & Homburg, 2004; Chmura, Anisfeld, Cahoon, & Lynch, 2003; Connor, Chmura, & Beecher, 2001; Gallagher, Reimold, Linthurst, & Pfeiffer, 1980). The productive capacity of tidal wetlands has often been compared to that of tropical evergreen rain forests (Choi & Wang, 2004; Pidgeon, 2009). However, these critical habitats are highly threatened by natural and anthropogenic activities such as global warming induced sea-level rise (Fitzgerald, Fenster, Argow, & Buynevich, 2008; Nicholls, Hoozemans, & Marchand, 1999), land use changes (Kennish, 2001; Silliman, Grosholz, & Bertness, 2009), soil erosion (Ravens, Thomas, Roberts, & Santschi, 2009; Sugumaran, Meyer, & Davis, 2004), natural and man-made disasters and associated clean-up efforts (Gilfillan et al., 1989; Hester & Mendelssohn, 2000; Mishra et al., 2012), and replacement by other species (Artigas & Pechmann, 2010).

A robust wetland monitoring program for sustainable management should be comprehensive in nature, covering various important

* Corresponding authors at: Department of Geography, University of Georgia, 210 Field Street, Room 204, Athens, GA 30602, USA.
*E-mail addresses:* shubho@uga.edu (S. Ghosh), dmishra@uga.edu (D.R. Mishra).

http://dx.doi.org/10.1016/j.rse.2015.11.015
0034-4257/

indicators such as distribution, composition, characteristics, health, and productivity (Adam, Mutanga, & Rugege, 2010; Mishra, Ghosh, Hladik, O'Connell, & Cho, 2015). However, traditional monitoring efforts, which rely on field sampling to study such wetland properties, are often costly, time consuming, and inadequate for analyzing the broad regional trends and spatio-temporal variability. Remote sensing using satellite and airborne sensors along with Geographic Information Systems (GIS) provides a cost-efficient alternative to intensive field surveys in monitoring and assessing coastal wetland ecosystems and their dynamics at different scales and resolutions (Dahl, 2006; Tiner, 1996).

In the last decade, advances in remote sensing technologies and increasing availability of high temporal and spectral resolution data, from both active and passive sensors, has significantly enhanced our ability to map wetland ecosystems (Evans & Costa, 2013; Jensen et al., 2007; Laba et al., 2008; Lefebvre, Corpetti, Bonnardot, Quénol, & Hubert-Moy, 2010; Wang, Christiano, & Traber, 2010; Zhang & Xie, 2012). Multi-temporal and multi-resolution imagery from sensors such as Landsat, Advanced Spaceborne Thermal Emission and Reflection Radiometer (ASTER), and Moderate Resolution Imaging Spectroradiometer (MODIS) are freely accessible to the general public and these sensors have been utilized in several studies for classification of wetland habitat (Campbell, 2007; Jensen, 2007; Lillesand, Kiefer, & Chipman, 2008). In addition, other moderate to high resolution satellite sensors such as SPOT, IKONOS, Quickbird, RapidEye, GeoEye, along with airborne hyperspectral imagers such as the Advanced Visible Infrared Imaging Spectrometer (AVIRIS) and Compact Airborne Spectrographic Imager (CASI), have been utilized by several researchers for classification of wetland cover and change detection analysis (Jensen, 1996; Rundquist, Narumalani, & Narayanan, 2001; Schmidt & Skidmore, 2003; Rosso, Ustin, & Hastings, 2005; Campbell, 2007; Lillesand, Kiefer, & Chipman, 2008; Gilmore et al., 2010; Klemas, 2011).

In general, wetland remote sensing is more challenging than remote sensing of terrestrial vegetation because the water or moist soil interface which reduces the intensity of the near-infrared (NIR) signal, shifts red-edge positions, and ultimately makes NDVI and red-edge-type indices less-sensitive to vegetation growth (Kearney, Stutzer, Turpie, & Stevenson, 2009; Turpie, 2013). These habitats also exhibit high spectral and spatial variation due to the abrupt change of environmental conditions that produce narrow ecotones, causing difficulty in vegetation community boundary identification (Schmidt & Skidmore, 2003). The diversity of vegetation in the wetland habitats produce unique species assemblages with different phenological cycles, morphological structures, and bio-chemical compositions, which, in turn, produces diverse spectral behavior, making mapping of wetlands difficult (Rosso et al., 2005; Zomer, Trabucco, & Ustin, 2009). A paucity of spectral library data is a challenge for wetland remote sensing because of species diversity (Zomer et al., 2009) and intraspecific morphologic differences. Further, the patchiness and fine scale heterogeneity of wetland vegetation are often not captured with medium resolution sensors such as Landsat and SPOT. High resolution aerial photography and imagery is expensive to acquire and labor intensive to process. On the other hand, classification using coarse resolution MODIS or Advanced Very High Resolution Radiometer (AVHRR) at 250–1000 m resolutions results in frequent misclassification of pixels (Friedl et al., 2002; Loveland et al., 1999).

The majority of research efforts for monitoring wetlands using remote sensing have been focused on delineating the extent of wetland ecosystems, and classifying plant communities using both active and passive satellite sensors and numerous image processing techniques (Adam et al., 2010; Artigas & Pechmann, 2010; Collin, Long, & Archambault, 2010; Davranche, Lefebvre, & Poulin, 2010; Filippi & Jensen, 2006; Gilmore et al., 2010; Goudie, 2013; Jensen et al., 2007; Klemas, 2011; Simard, Fatoyinbo, & Pinto, 2010; Wang, 2010). This kind of mapping provides crucial information regarding the presence/absence of wetland patches, the previous and current spatial extent, and the dynamics of wetland cover change. However, it does not provide any information regarding the biophysical characteristics which are primary indicators of tidal wetlands' physiological status, photosynthetic capacity as well as, chlorophyll and nitrogen content (CHL, N). Remote estimation of biophysical characteristics such as Leaf Area Index (LAI), Canopy Chlorophyll Content ($CHL_c$), vegetation fraction (VF), and Above Ground Green Biomass (GBM) should be performed regularly to assess the health of the wetland ecosystem.

Over the past twenty years, studies have focused on protocols for mapping the biophysical characteristics of terrestrial vegetation, using both *in situ* and satellite based surface reflectance. LAI mapping from spectral reflectance measurements has mainly focused on forests (e.g. Gong, Pu, & Miller, 1995; Davi et al., 2006) and crops (Hansen & Schjoerring, 2003; Pay, Das, Singh, & Panigrahy, 2006; Thenkabail, Smith, & De Pauw, 2000). Developing regression based models with vegetation indices (VIs) such as NDVI and simple ratio, which are derived from visible and NIR wavelengths, has been the most widely used empirical model for estimating LAI (Thenkabail et al., 2000; Gong et al., 1995; Kovacs, Wang, & Flores-Verdugo, 2005). Similar research studies have also been performed for estimating GBM using satellite derived VIs (Proisy, Couteron, & Fromard, 2007; Rendong & Jiyuan, 2004). Apart from LAI and GBM, mapping CHL content through non-invasive techniques in terrestrial vegetation has been attempted often (Gamon & Surfus, 1999; Gitelson, Keydan, & Merzlyak, 2006; Gitelson & Merzlyak, 1994; Markwell, Osterman, & Mitchell, 1995; Richardson, Duigan, & Berlyn, 2002). Finally, *in situ* reflectance and satellite derived VIs have been used for monitoring fractional cover of green vegetation, using different combinations of visible and NIR bands (Gitelson, 2004; Gitelson, Kaufman, & Merzlyak, 1996; Gitelson, Kaufman, Stark, & Rundquist, 2002b; Gitelson et al., 2002a; Myneni, Keeling, Tucker, Asrar, & Nemani, 1997a; Myneni, Nemani, & Running, 1997b).

However, remote sensing studies focusing on monitoring and analyzing the biophysical properties of tidal wetland ecosystems are very limited, and have only been attempted using satellite sensors with coarse temporal resolution. (e.g. Hardisky, Daiber, Roman, & Klemas, 1984; Jensen, Rutchey, Koch, & Narumalani, 2002; Kearney et al., 2009; Mishra et al., 2012). These studies on tidal wetlands have mostly been conducted using traditional field sampling methods (Darby & Turner, 2008; Hopkinson, Gosselink, & Parrando, 1978; Stout, 1984). Although these studies provide in-depth site-specific information of biophysical characteristics, they often lack the ability to provide insight into the long-term spatio-temporal trends of the tidal wetlands at a landscape scale. Monitoring biophysical properties using remote sensing not only helps in assessing the overall dynamics of wetlands but also facilitates prioritization of restoration efforts to areas that require immediate attention and allows conservation planning at a much broader spatial scale. A robust biophysical mapping protocol is also critical in assessing the success or failure of previous restoration efforts (Friess et al., 2012; Hinkle & Mitsch, 2005), as well as analysis of phenology and carbon budgets at regional and global scales across a wide range of ecosystem and climatic regimes (Baldocchi, 2003; Churkina, Schimel, Braswell, & Xiao, 2005; Richardson, Braswell, Hollinger, Jenkins, & Ollinger, 2009). For example, analysis of the biophysical characteristics based phenology can aid in isolating the natural variability in wetlands from the variability introduced by environmental forcings such as localized drought, dieback events, or hurricanes. Furthermore, remote assessment of gross primary productivity (GPP) can be performed using these biophysical characteristics; and that is the long-term goal of our research.

The specific objectives of this research were to (1) calibrate and validate MODIS based VIs for estimating the tidal wetland biophysical characteristics (GLAI, $CHL_c$, VF, GBM) in the northern Gulf of Mexico (GoM), (2) develop time-series composites of tidal wetland biophysical characteristics for long-term productivity trend analysis, and (3) analyze broader phenological patterns of the biophysical characteristics to assess the impact of various natural and anthropogenic disasters. The novelty of this research is that it will allow researchers and coastal

managers to use high frequency MODIS data to study the biophysical characteristics of tidal wetland habitats in the Gulf Coast, for the first time. This study has the potential of increasing our predictive capability with respect to carbon sequestration in these ecosystems. In addition, an efficient and non-destructive MODIS based biophysical mapping protocol for emergent wetlands will be an invaluable tool for frequent monitoring as well as conservation and restoration decision making.

## 2. Study area

Tidal wetlands cover more than 8500 sq. km of the coastal areas of the Northern GoM (Source: http://www.fws.gov/wetlands/) (Fig. 1). The tidal marsh habitats are mostly dominated by smooth cord-grass (*Spartina alterniflora*), salt meadow cord-grass (*Spartina patens*), and black needle rush (*Juncus roemarianus*). Patchy distributions of American Glasswort (*Salicornia virginica*), saltwort (*Batis maritima*), and seashore saltgrass (*Distichlis spicata*) are also encountered. The highly saline and anoxic nature of the soil inhibits the growth of non-specialized plants; as such, floral diversity is remarkably low (Weis, 2010). Average annual temperature in this region varies between 15 and 25 °, while annual precipitation ranges from 80 to 100 cm (National Weather Service, http://www.weather.gov/).The region experiences tropical to sub-tropical climate characterized by hot and humid summers, with occasional tropical storms and moderately cold winters. In the last decade, the tidal wetland habitats in the Gulf have experienced the landfall of major hurricanes, such as Lili (2002), Katrina and Rita (2005), Gustav (2008), Ida (2009), and Isaac (2012) in Louisiana (LA) and Gordon (2000), Gabrielle (2001), Ivan (2004), and Dennis (2005) in Florida (FL) (National Hurricane Centre, http://www.nhc.noaa.gov/). LA has the largest tidal wetland extent among all the Gulf Coast states. However, the marshes here are also home to more than 160,000 oil and gas wells (Lyles, Namwamba, & Campus, 2005), accounting for 18% of oil and 24% of natural gas production in the U.S., valued at $6.3 billion, and $10.3 billion respectively (Tiner, 2013). As such, the marshes have been subjected to intense dredging and channelization for transportation as well as significant groundwater removal, which has led to soil and marsh erosion and localized subsidence. Further, the sediment flow from the Mississippi River, which typically provides nutrients and substrate for tidal wetlands, has been extensively trapped through excessive construction of levees across the LA coast. Hence, it is increasingly difficult for the tidal wetlands to sustain themselves. Disturbed tidal wetland habitats in the region have been invaded by common reed (*Phragmites australis*) (Tiner, 2013). The marshes in FL have also been subjected to channelization, with excavated materials being dumped into the confined disposal areas within tidal wetlands (Tiner, 2013).

Over the past decade, there have been an increasing number of reports of tidal wetland "dieback" in the U.S. In 2000 and 2007, LA experienced a sudden and acute dieback event (termed "brown marsh") that affected over 100,000 ha of *Spartina alterniflora* dominated tidal wetland throughout the Mississippi River deltaic plain (Bertness, Silliman, & Holdredge, 2009; Lindstedt & Swenson, 2006). In addition, although the long-term impact is still unknown, the Deepwater Horizon oil spill in 2010 had a severe short-term impact on the health of several fringe and interior tidal wetland patches of LA, MS, and AL characterized by loss of chlorophyll, biomass, and subsequently a reduction in photosynthetic capacity (Biber, Wu, Peterson, Liu, & Pham, 2012; Mishra et al., 2012; Mishra et al., 2015 (in press)). Therefore, this research is aimed at fulfilling the strong need to develop an accurate and non-destructive mapping protocol that uses high temporal resolution satellite data to frequently monitor the biophysical conditions of these vast patches of tidal emergent wetlands of the Gulf Coast at a broad scale.

## 3. Methods

### 3.1. Field data collection

The models developed for mapping tidal wetland biophysical characteristics were based on establishing statistical relationships between MODIS 250 m and 500 m surface reflectance products and on-field estimates of these characteristics. Therefore, extensive fieldwork was conducted in four Gulf States (Louisiana (LA); Mississippi (MS); Alabama (AL); Florida (FL)) during the tidal wetland growing season (May–October) of 2010 and 2011. The field data collection involved acquisition of top of canopy hyperspectral reflectance and biophysical characteristics *viz.* LAI, VF, $CHL_l$ (Leaf Chlorophyll Content), and GBM, from numerous study plots. Field sites were selected in areas with extensive homogenous patches of marsh potentially covering multiple MODIS (250 m and 500 m) pixels. The site selection process involved analysis of high resolution satellite data (Landsat, QuickBird, and Google Earth), short field visits, aerial surveys, reconnaissance surveys, and in consultation with state and local officials. Multiple calibration and validation sites were selected across coastal counties covering the four Gulf States. Within each 250 m or 500 m MODIS pixel, multiple (~4–8) mono-specific sub-plots were selected for field data acquisition based on accessibility. Few pixels with single study plots were also incorporated in the analysis, after visual estimation of spatial homogeneity from aerial photographs and Google Earth images. Care was taken to make sure that the sub-plots were as homogenous as possible with similar health conditions and growth stages (Table 1). The data from all the sub-plots within a specific site were aggregated to represent a MODIS

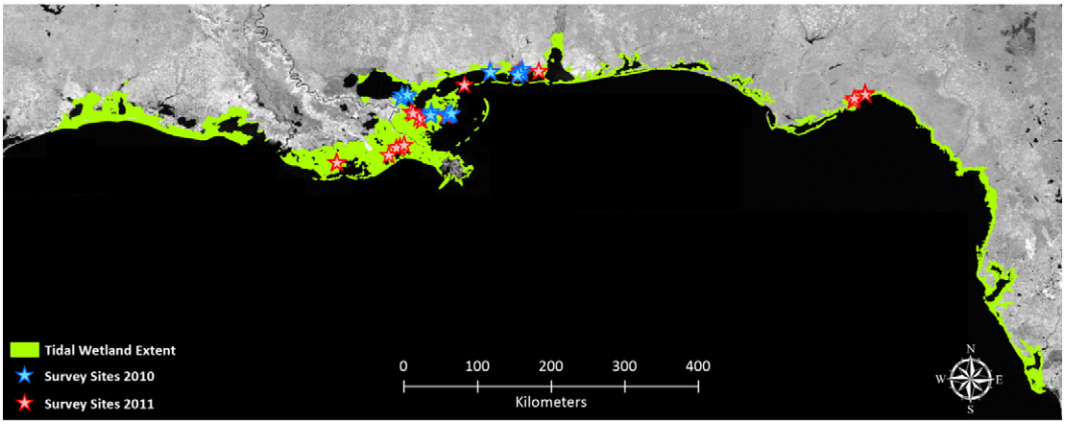


**Fig. 1.** Map showing salt marsh extent in northern Gulf of Mexico, with survey sites for 2010 and 2011. Each of the survey sites contained numerous sub-plots from where the detailed field data were acquired.

**Table 1**
Detailed information on study sites used for MODIS model calibration and validation, with number of study plots in each site and number of corresponding usable MODIS 250 m and 500 m pixels. Pixel center coordinates for 250 m data is provided. 500 m pixels can also be accessed with the provided co-ordinates.

| Data | State | Site | Month | Year | No. of plots | Species | No. of usable MODIS pixels | | Pixel Center Coordinates for 250 m (Approx.) |
|---|---|---|---|---|---|---|---|---|---|
| | | | | | | | 250 m | 500 m | |
| Calibration | Louisiana | Bayou Savage | August | 2010 | 7 | *Spartina, Juncus* | 7 | 7 | 30.09, −89.8; 30.07, −89.79; 29.88, −89.51; 29.86, −89.51; 29.86, −89.52; 29.85, −89.52; 29.85, −89.51 |
| | Mississippi | Marsh Point | September | 2010 | 20 | *Spartina, Juncus, Distichlis* | 3 | 2 | 30.37, −88.79; 30.38, −88.79; 30.38, −88.78 |
| | Louisiana | Plaquemine/Terreborne parish | September | 2010 | 25 | *Spartina, Salicornia, Distichlis* | 3 | 1 | 29.87, −89.26; 29.86, −89.31; 29.84, −89.3 |
| | Mississippi | Marsh Point | September | 2010 | 5 | *Spartina* | 1 | 1 | 30.36, −88.79 |
| | Mississippi/Alabama | Grand Bay | October | 2010 | 37 | *Spartina, Salicornia, Distichlis, Juncus* | 5 | 5 | 30.34, −88.45; 30.33, −88.45; 30.36, −88.42; 30.37, −88.4; 30.41, −88.4 |
| Validation | Mississippi/Alabama | Grand Bay | May | 2011 | 44 | *Spartina, Salicornia, Distichlis, Juncus* | 7 | 7 | 30.36, −88.42; 30.35, −88.39; 30.39, −88.41; 30.35, −88.45; 30.35, −88.46; 30.33, −88.45; 30.38, −88.43 |
| | Louisiana | Plaquemine/Terreborne parish | June | 2011 | 21 | *Spartina, Salicornia, Distichlis* | 4 | 3 | 29.81, −89.66; 29.77, −89.63; 29.83, −89.33; 29.84, −89.33 |
| | Mississippi | Marsh Point/Cat Island | July | 2011 | 10 | *Spartina, Juncus* | 5 | 2 | 30.21, −89.11; 30.38, −88.79; 30.11, −84.21; 30.11, −84.2; 30.09, −84.2 |
| | Florida | St Marks | August | 2011 | 16 | *Juncus* | 4 | 2 | 30.09, −84.21; 30.05, −84.34; 30.02, −84.36; 30.02, −84.35 |

pixel during model calibration and validation. The detailed collection protocol for each field dataset is provided below.

*3.1.1. Top of canopy reflectance (ρ)*

A dual-fiber system, with two inter-calibrated Ocean Optics USB4000 hyperspectral radiometers (Ocean Optic Inc., Dunedin, FL, USA), mounted on an aluminum frame was used to acquire the top of canopy (TOC) spectral reflectance ($R_{rs}$, $sr^{-1}$) data in the range of 200–1100 nm with a sampling interval of 0.3 nm (Rundquist, Perk, Leavitt, Keydan, & Gitelson, 2004). The first radiometer with a field-of-view (FOV) of 25° pointed downwards to acquire upwelling radiance ($L$; $Wm^2sr^{-1}$), while the second radiometer equipped with a cosine corrector pointed upward to simultaneously acquire downwelling irradiance ($E$; $Wm^{-2}$). Based on the FOV and the height of the frame (5 m), the spatial resolution (IFOV) of the sensor was calculated to be 1.83 m (Fig. 2a and b).

$$d = 2\{h \times \left(tan\frac{\infty}{2}\right) \quad (1)$$

where, $d$ = diameter of the IFOV (m), $h$ = height of the sensor from the target (m), $\alpha$ = FOV of the sensor (degree). Inter-calibration of the radiometers was accomplished by measuring the $L$ and $E$ of a 99% Spectralon white polytetrafluoroethylene (PTFE) reflectance panel (Labsphere, Inc., North Sutton, NH, USA) (Rundquist et al., 2004). To mitigate the impact of solar elevation on radiometer inter-calibration, the anisotropic reflectance from the calibration target was corrected in accordance with Jackson et al. (1992). Data were collected with the sensors configured to take 15 simultaneous $L$ and $E$ measurements, which were internally averaged and stored as a single data file. In case of changing sky conditions, the sensor was recalibrated at regular intervals (Fig. 2c and d). The hyperspectral readings were smoothed using a moving window average of 7 nm to eliminate noise and then further interpolated at a 1 nm interval. The four scans of radiance and irradiance acquired per sub-plot were converted to four $R_{rs}$ readings by dividing $L$ over $E$; percentage spectral reflectance (ρ) was estimated and then averaged out to obtain composite spectra of the sub-plot.

*3.1.2. Above-ground green biomass (GBM)*

GBM data were collected by destructive sampling from a 0.09 $m^2$ (1 $ft^2$) representative area within each sub-plot using a PVC frame and clippers (Fig. 2e and f). Each biomass sample was sorted to separate the green from brown (standing dead), oven dried at 65 °C overnight (~24 h) to get rid of any moisture, and then the dry weight was recorded using a standard measuring balance. Vegetation samples, mainly *Salicornia* and *Batis*, which showed presence of moisture, even after 24 h of drying, were further dried for additional 24 h, until all moisture was eliminated. Precautions were taken to avoid moisture absorption by the dried GBM during dry weight measurement. The dry GBM weights were then rescaled from gram dry weight per square feet ($gft^{-2}$) to gram dry weight per square meter ($gm^{-2}$).

*3.1.3. Leaf chlorophyll content ($CHL_l$)*

A Minolta 502 SPAD Chlorophyll meter (Spectrum Technologies Inc., East Plainfield, IL, USA) was used to measure the *in situ* $CHL_l$ (Fig. 2g). A total of twenty stratified random SPAD readings were acquired from each sub-plot across varying CHL levels inside the IFOV of the sensor. Conversion of SPAD readings to actual $CHL_l$ was done by establishing a linear relationship between SPAD values and corresponding CHL estimated through chemical extraction and spectrophotometric measurements. The CHL extraction procedure used in this research has been described in details by Biber (2007). For this study, leaf samples of *Spartina, Juncus, and Distichlis,* showing varying degrees of greenness (from dark green to almost yellow/brown) were collected from the study plots. 5 cm long sections from the basal portion of the leaves were used for CHL extraction. Three SPAD readings were taken from selected sections on the leaves and averaged. These averaged SPAD values were then calibrated against chemically extracted CHL from

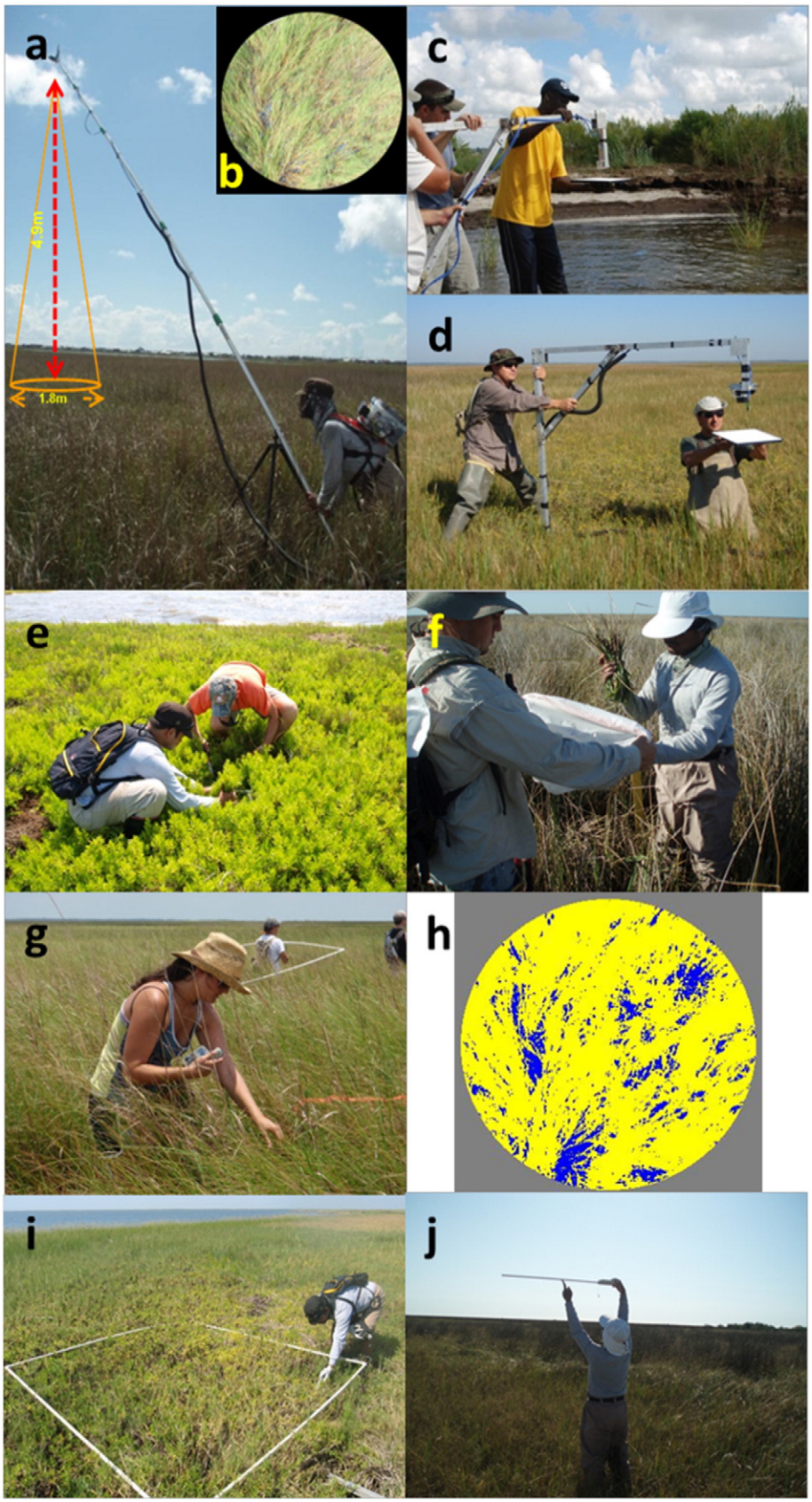


**Fig. 2.** *In situ* data collection activities at each sub-plot; a: Spectral reflectance acquisition using Ocean Optics sensor; b: Sensor altitude (4.9 m) and IFOV (1.8 m); c and d: Sensor calibration using a Labsphere 99% reflectance spectralon panel; e and f: Biomass collection from sub-plot; g: Leaf chlorophyll content (Chl) measurement using SPAD 502 chlorophyll meter; h: Vegetation fraction binary mask measured from the IFOV of the sensor using a digital camera; i and j: LAI measurements using LICOR LAI Plant Canopy Analyzer 2000 and AccuPAR LP-80 Ceptometer.

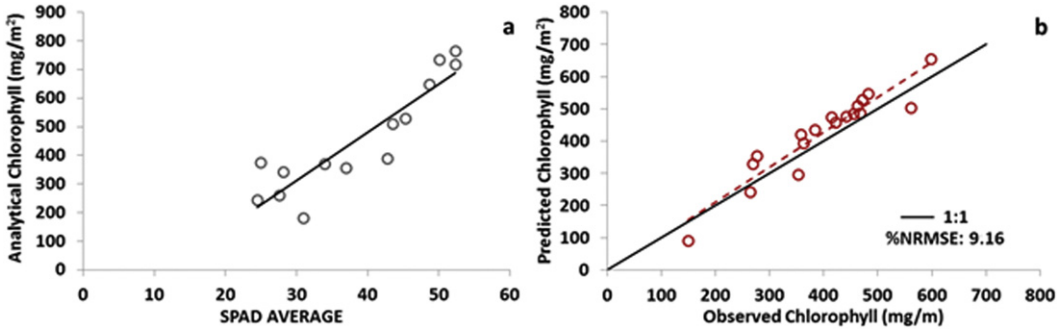


**Fig. 3.** a. Relationship between SPAD readings acquired at each sub-plot calibrated against analytical chlorophyll content values from laboratory analysis; b. Validation of the SPAD model showing % NRMSE and 1:1 line.

those sections using the following equation:

$$CHL_l\ (mgm^{-2}) = SPAD \times 16.844 - 192.84. \quad (2)$$

Separate datasets were used for calibration and validation (14 readings for calibration and 18 for validation). The linear model between SPAD and analytically extracted chlorophyll content showed a percent normalized root mean square error (%NRMSE; described later in the article) of 9% (Fig. 3a and b).

### 3.1.4. Vegetation fraction (VF)

Percentage green VF was estimated from a circular crop of vertical digital photographs of the study plots acquired by OLYMPUS E-400 digital SLR camera (Olympus America Inc., Centre Valley, PA, USA). The camera was installed on the frame along with a laser pointer next to the hyperspectral radiometer. The laser pointer marked the center of the digital photograph and the IFOV of the hyperspectral radiometer. The digital photograph was cropped to match the IFOV of the hyperspectral radiometer and a simple pixel count code was implemented to count the total pixels and green pixels in the cropped photographs. VF (%) was estimated by the ratio of the number of green pixels to the total number of pixels in each photograph (Fig. 2h) (White, Asner, Nemani, Privette, & Running, 2000).

### 3.1.5. Leaf area index (LAI)

Leaf area index (LAI) was measured from each sub-plot using a LAI Plant Canopy Analyzer 2000 (LAI 2000; LICOR Biosciences Inc., Lincoln, NE, USA) (Nackaerts, Coppin, Muys, & Hermy, 2000) and AccuPAR LP-80 Ceptometer (Decagon Devices Inc., Pullman, WI, USA) (Delalieux et al., 2008; Kovacs, King, & de Santiago, 2009) (Fig. 2i and j). The average value of four LAI readings taken within each sub-plot was used as the representative LAI. Each LAI measurement involved one above-canopy and four below canopy readings. Both LAI 2000 and AccuPAR measure canopy transmittance for estimating LAI and as such, do not differentiate between green and dead leaves. LAI 2000 has an optical filter, which rejects any radiation above 490 nm; the assumption behind this is that foliar transmission is minimal in the blue region of the electromagnetic spectrum (LiCOR Inc., 2000). AccuPAR on the other hand, measures radiation transmitted through the canopy and scattered by leaves within the canopy. It is also assumed that the leaf absorptivity is maximum in the visible region of the electromagnetic spectrum (approximately 90% in the blue and red and 75–80% in the green region), thereby, assuming transmittance through leaves to be negligible (Decagon Devices, 2008). Based on these aforementioned assumptions, leaves are considered to be opaque, and as such, none of these instruments can differentiate between green and dead/yellow leaves.

Estimated LAI values, therefore, are a metric of total leaf area rather than green LAI. As the productive capacity of vegetation depends largely on the presence of green foliage containing CHL, Green Leaf Area Index (GLAI) serves as a better estimate of the vegetation health. Since VF is an estimate of the amount of greenness in the area of interest, we estimated Green LAI as the product of LAI and VF. Further, $CHL_c$ ($mgm^{-2}$) was calculated as the product of LAI and $CHL_l$ content (Gitelson, Vina, Ciganda, Rundquist, & Arkebauer, 2005).

$$GLAI = LAI \times VF \quad (3)$$

$$CHL_c\ (mgm^{-2}) = CHL_l\ (mgm^{-2}) \times LAI \quad (4)$$

### 3.2. Satellite data

Multi-temporal 8-day Level 1B atmospherically corrected surface reflectance composites for the northern GoM (LA, MS, AL, and western FL coast) were acquired from National Aeronautics and Space Administration (NASA) website (http://modis-land.gsfc.nasa.gov) for the years 2000 through 2014. Both 250 m and 500 m scenes from MODIS sensor (MOD09Q1 and MOD09A1 respectively) were downloaded for the northern GoM and mosaicked. The mosaic scenes were cropped to isolate the tidal wetland habitats by using the most recent vector boundaries obtained from NWI database (http://www.fws.gov/wetlands/). The aforementioned pre-processing of the MODIS images was performed using ERDAS Imagine 2013 (ERDAS Imagine, Intergraph Corporation Part of Hexagon, Norcross, GA). We used the MODIS

**Table 2**
Summary statistics for the field data collected over growing seasons of 2010 and 2011, along with respective MODIS 250 m and 500 m pixel averages for each biophysical parameter.

| Year | | Raw data | | | | MODIS pixel average (250 m) | | | | MODIS pixel average (500 m) | | | |
|---|---|---|---|---|---|---|---|---|---|---|---|---|---|
| | | GBM | VF | GLAI | CHL | GBM | VF | GLAI | CHL | GBM | VF | GLAI | CHL |
| 2010 | Max | 6094.53 | 98.75 | 1.87 | 1242.61 | 1091.77 | 97.46 | 1.79 | 842.71 | 1102.17 | 98.52 | 1.87 | 906.02 |
| | Min | 42.61 | 0.30 | 0.001 | 0.77 | 104.57 | 0.34 | 0.001 | 158.93 | 308.66 | 2.09 | 0.09 | 1.15 |
| | Mean | 858.42 | 44.78 | 0.53 | 321.10 | 714.68 | 55.33 | 0.81 | 522.27 | 694.74 | 53.14 | 0.81 | 278.67 |
| | St. Dev | 811.32 | 28.83 | 0.51 | 276.35 | 273.45 | 26.71 | 0.57 | 217.28 | 290.21 | 33.26 | 0.68 | 311.42 |
| 2011 | Max | 2422.20 | 95.01 | 3.54 | 1603.58 | 827.02 | 75.83 | 1.78 | 739.86 | 841.31 | 55.81 | 1.53 | 723.51 |
| | Min | 115.28 | 2.09 | 0.001 | 40.83 | 268.34 | 29.13 | 0.24 | 273.46 | 322.59 | 8.35 | 0.30 | 268.09 |
| | Mean | 579.04 | 32.27 | 1.05 | 521.94 | 584.04 | 51.17 | 0.89 | 473.25 | 582.73 | 37.56 | 0.92 | 457.14 |
| | St. Dev | 330.01 | 20.81 | 0.85 | 383.70 | 181.38 | 17.01 | 0.48 | 157.42 | 154.91 | 14.33 | 0.50 | 133.93 |

**Table 3**
List of satellite image derived VIs used for calibration and validation of the wetland biophysical characteristics.

| Vegetation index | Formula | Reference |
|---|---|---|
| Normalized difference vegetation index (NDVI) | $(R_{NIR} - R_{red})/(R_{NIR} + R_{red})$ | Rouse et al., 1974 |
| Enhanced vegetation index 2 (EVI2) | $\{2.5 \times (R_{NIR} - R_{red})/(R_{NIR} + 2.4 \times R_{red} + 1)\}$ | Huete et al., 2002 |
| Chlorophyll index red ($CI_{red}$)[a] | $(R_{NIR} - R_{red})/R_{red}$ | Gitelson et al. 2006 |
| Wide dynamic range vegetation index (WDRVI) | $(\alpha \times R_{NIR} - R_{red})/(\alpha \times R_{NIR} + R_{red})$ | Gitelson, 2004 |
| Soil adjusted vegetation index (SAVI) | $(R_{NIR} - R_{red}) \times (I + L)/(R_{NIR} + R_{red} + L)$ | Huete, 1988 |
| Chlorophyll index green ($CI_{green}$) | $(R_{NIR} - R_{green})/R_{green}$ | Gitelson et al., 2006 |
| Green normalized difference vegetation index (GNDVI) | $(R_{NIR} - R_{green})/(R_{NIR} + R_{green})$ | Gitelson et al., 1996c |
| Visible atmospherically resistant index (VARI) | $(R_{green} - R_{red})/(R_{green} + R_{red})$ | Gitelson et al., 2002a |

[a] $R_{red}$ was used instead of $R_{red\text{-}edge}$ as described in Gitelson et al. (2006).

Quality Assurance (QA) layer for both 250 m and 500 m data to select the highest quality pixels. The QA layers for 250 m and 500 m are 16-bit and 32-bit images, respectively, representing different permutations and combinations of MODIS land surface reflectance quality parameters. We chose the best combination of bits, e.g. 00 for both clouds and cloud shadows, 0000 for highest data quality for all the bands, 0 for both snow cover and fire, 0 for internal cloud, fire and snow algorithm, and 1 for atmospheric, adjacency and bi-directional reflectance function (BDRF) corrections to eliminate pixels affected by various natural and technical factors such as cloud cover, cloud shadows, atmospheric noise, snow cover, fire, sensor orbits, cloud adjacency, bi-directional reflection, sensor failure etc. (Vermote, Kotchenova, & Ray, 2011). Summary statistics for all the biophysical characteristics field data and coincident MODIS pixel data for 2010 and 2011 is provided in Table 2.

## 4. Analysis

### 4.1. Tidal wetland spectral response: In situ and MODIS

In order to analyze the difference in reflectance magnitude and the effect of species variability, MODIS and Ocean Optics derived *in situ* ρ data were compared. ρ values of both 250 m and 500 m MODIS surface reflectance products from *Spartina* and *Juncus* dominated pixels were extracted for all sites where Ocean Optics ρ data were acquired. *Salicornia* and *Distichlis* had patchy distributions; as such no homogenous MODIS pixels of these two species were found. Since plot level data for these two species were very limited ($n < 5$), spectral response comparison between Ocean Optics and MODIS was limited to the dominant species (*Spartina* and *Juncus*) only. The Ocean Optics acquired data were further integrated to match the MODIS VNIR bandwidths. Ocean Optics spectra obtained for *Spartina* and *Juncus*, were averaged for the sites falling within one MODIS pixel (for both 250 m and 500 m), for accurate comparison between ground level and satellite level reflectance. As such, we used two visually mono-specific pixels (from both 250 m and 500 m images) for each species (*Spartina* and *Juncus*). Average hyperspectral ρ acquired using Ocean Optics data from mono-specific study plots within these MODIS pixels were compared with MODIS derived ρ.

### 4.2. Model calibration and validation

The main goal of model calibration was to establish relationships between several well established VIs and wetland biophysical

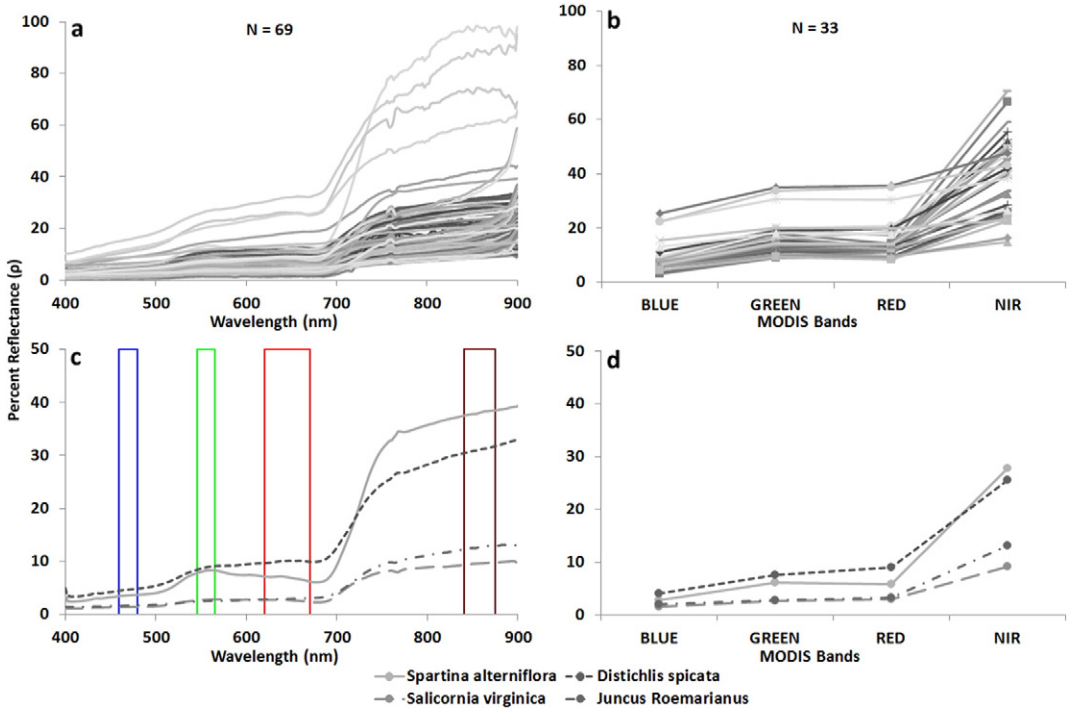


**Fig. 4.** a. Reflectance (%) spectra of 69 sub-plots covering multiple species acquired using Ocean Optics sensor. b. Reflectance (%) spectra derived from MODIS 8-day 500 m surface reflectance images for 33 pixels containing the study plots from 2010 to 2011. c. Sample spectra for individual species as acquired by the *in situ* sensor with highlighted MODIS bandwidths. Differences in the species level spectral response pattern were mainly due to the variability in canopy structure and chlorophyll content. d. Sample spectra acquired using Ocean Optics sensor for individual species averaged to MODIS bandwidths. Differences in species specific spectral response were clearly visible similar to the *in situ* reflectance profile.

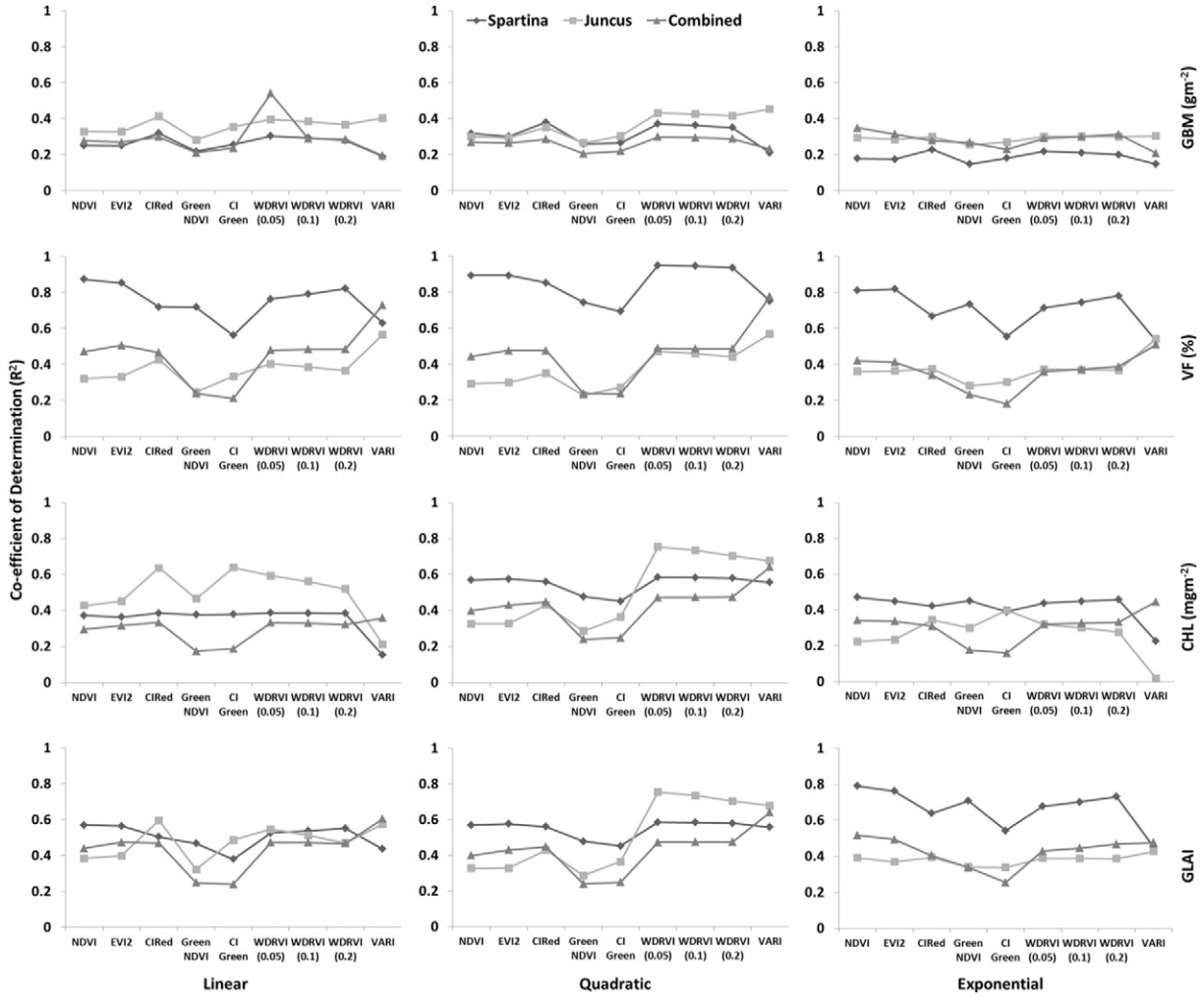


**Fig. 5.** Coefficient of determination values of species specific and species invariant linear, quadratic, and exponential relationships between VIs and (a, e, i): GBM, (b, f, j): VF, (c, g, k): CHL and (d, h, i): GLAI, respectively developed from *in situ* sensor derived VIs.

characteristics. Then established models were validated using MODIS data. These VIs have been widely used at fine and coarse spatial resolutions to monitor terrestrial vegetation biophysical characteristics, both at site specific and broader ecosystem scales. However, these indices have not been used at the MODIS scale to map biophysical characteristics such as GLAI, CHL, GBM, and VF of tidal wetlands so far. It has not been done because collecting accurate, long-term, and representative biophysical data for MODIS based VI calibration for wetland ecosystems

**Table 4**
Pearson's rank correlation between biophysical characteristics and Ocean Optics derived VIs for Spartina, Juncus, all homogenous and heterogenous plots.

| Pearson's Rank Correlations | | NDVI | EVI2 | WDRVI ($\alpha = 0.1$) | WDRVI ($\alpha = 0.2$) | $CI_{red}$ | SAVI | G NDVI | $CI_{green}$ | VARI |
|---|---|---|---|---|---|---|---|---|---|---|
| Spartina (N = 19) | GBM | **0.502** | **0.5** | **0.542** | **0.529** | **0.566** | **0.478** | **0.467** | **0.507** | .436 |
| | VF | 0.934 | 0.923 | 0.889 | 0.907 | 0.849 | 0.936 | 0.847 | 0.75 | 0.794 |
| | CHL | 0.611 | 0.603 | 0.622 | 0.62 | 0.621 | 0.594 | 0.613 | 0.616 | .392 |
| | GLAI | 0.754 | 0.751 | 0.733 | 0.742 | 0.71 | 0.758 | 0.683 | 0.616 | 0.66 |
| Juncus (N = 13) | GBM | **0.573** | **0.573** | **0.62** | **0.606** | **0.642** | 0.546 | .532 | **0.596** | **0.635** |
| | VF | **0.567** | **0.576** | **0.622** | **0.604** | **0.653** | **0.556** | .497 | **0.578** | 0.752 |
| | CHL | **0.654** | **0.672** | 0.75 | 0.721 | 0.798 | **0.632** | **0.683** | 0.799 | .462 |
| | GLAI | **0.619** | **0.632** | 0.716 | 0.685 | 0.772 | **0.591** | **0.568** | 0.698 | 0.758 |
| All Homogenous (N = 42) | GBM | 0.565 | 0.557 | 0.576 | 0.572 | 0.581 | 0.547 | 0.494 | 0.519 | 0.489 |
| | VF | 0.706 | 0.73 | 0.714 | 0.715 | 0.702 | 0.732 | 0.521 | 0.493 | 0.861 |
| | CHL | 0.544 | 0.562 | 0.574 | 0.568 | 0.578 | 0.552 | 0.418 | 0.433 | 0.599 |
| | GLAI | 0.678 | 0.703 | 0.703 | 0.699 | 0.702 | 0.698 | 0.524 | 0.516 | 0.788 |
| Heterogenous (N = 22) | GBM | 0.053 | 0.057 | 0.053 | 0.054 | 0.051 | 0.058 | −0.120 | −0.084 | **0.492** |
| | VF | 0.218 | 0.217 | 0.178 | 0.194 | 0.138 | 0.230 | 0.009 | −0.008 | 0.603 |
| | CHL | 0.292 | 0.278 | 0.265 | 0.275 | 0.240 | 0.278 | 0.151 | 0.135 | **0.443** |
| | GLAI | 0.326 | 0.317 | 0.281 | 0.299 | 0.238 | 0.325 | 0.049 | 0.050 | 0.798 |

Values in bold indicate significant correlation at 0.05 level.

**Table 5**
Linear $R^2$ for MODIS (250 m) derived VIs calibrated against different biophysical characteristics. Because of the similarity in performance of all the red-NIR based VIs, it was not possible to determine the best model for the 250 m data from the $R^2$ table alone. Best model selection was therefore dependent on the analysis of other parameters such as %NRMSE, slope ratio, and residual trends as explained in Section 5.3.

| $R^2$ | NDVI | EVI2 | $CI_{red}$ | WDRVI ($\alpha = 0.1$) | WDRVI ($\alpha = 0.2$) | SAVI |
|---|---|---|---|---|---|---|
| GLAI | 0.867 | 0.865 | 0.770 | 0.821 | 0.846 | 0.867 |
| VF (%) | 0.864 | 0.868 | 0.811 | 0.845 | 0.859 | 0.864 |
| GBM ($gm^{-2}$) | 0.864 | 0.871 | 0.819 | 0.850 | 0.864 | 0.864 |
| CHL ($mgm^{-2}$) | 0.811 | 0.837 | 0.813 | 0.837 | 0.843 | 0.811 |

**Table 6**
Linear %NRMSE values for MODIS (250 m) derived biophysical models for different biophysical characteristics. Relative high %NRMSE corresponding to high $R^2$ (NDVI, EVI2 and SAVI; from Table 4) signifies inherent bias in the model or non-uniform sensitivity of the indices to biophysical characteristics.

| % NRMSE | NDVI | EVI2 | $CI_{red}$ | WDRVI ($\alpha = 0.1$) | WDRVI ($\alpha = 0.2$) | SAVI |
|---|---|---|---|---|---|---|
| GLAI | 19.165 | 17.443 | 14.030 | 14.967 | 15.957 | 19.168 |
| VF (%) | 25.163 | 23.659 | 21.538 | 22.055 | 22.636 | 25.163 |
| GBM ($gm^{-2}$) | 19.504 | 19.355 | 20.151 | 19.616 | 19.425 | 19.505 |
| CHL ($mgm^{-2}$) | 26.297 | 25.913 | 26.052 | 25.817 | 25.789 | 26.292 |

is an extremely difficult task. Inaccessible areas in difficult terrain, unavailability of large visually homogenous patches of mono-specific wetland vegetation, poor sampling design and improper *in situ* data collection procedure often limit large scale remote sensing studies on wetland biophysical characteristics. In this study, an extensive and comprehensive *in situ* data collection over a period of two years enabled us to perform a comparative assessment of the existing VIs which is crucial for providing insight into both selection of the best VI for mapping wetland biophysical characteristics, and the possible explanation for their respective performances.

#### 4.2.1. Using in situ hyperspectral data

*In situ* ρ spectra were collected for the growing season (April–October) of 2010, from 42 mono-specific and 22 multi-specific but visually homogenous study plots. Several well established VIs (Table 3) were derived from Ocean Optics ρ, and used for initial calibration against the biophysical characteristics using SPSS (SPSS IBM, New York, USA). Among these VIs, Normalized Difference Vegetation Index (NDVI), Enhanced Vegetation Index (EVI2), Chlorophyll Index ($CI_{red}$), Wide Dynamic Range Vegetation Index (WDRVI), and Soil Adjusted Vegetation Index (SAVI) were developed utilizing reflectance at red and NIR bands. $CI_{red}$ is a modified (from Chlorophyll Index red edge or $CI_{red\text{-}edge}$) chlorophyll index, using the red band instead of the red edge band (Gitelson et al., 2006). Visible Atmospherically Resistant Index (VARI) was developed using the visible green and red bands (Gitelson et al., 2002b, 2002a).

Variability in spectral response is unavoidable in the tidal wetland landscape because of wetlands' variability in terms of species composition, leaf and canopy structure, chlorophyll content, phenological stage, standing dead matter, and substrate nature. Therefore, species-specific models for biophysical mapping might account for this variability, and subsequently assist in the development of a robust method for mapping of biophysical characteristics. Therefore, both linear and non-linear (quadratic and exponential) biophysical models were calibrated for individual species using *in situ* Ocean Optics hyperspectral data. Coefficient of determination ($R^2$) was derived for species-specific biophysical models and also for a species-independent model combining all species data. However, since *Salicornia* and *Distichlis* had patchy occurrences, there were not enough mono-specific plots for these two species for reasonable calibration ($n < 5$). Therefore, species-specific models were analyzed for only the two dominant species: *Spartina* and *Juncus*.

#### 4.2.2. Using MODIS data

Following the initial pre-processing of MODIS data, *in situ* sampling locations were used do extract pixel values from MODIS images. Scenes were chosen based on the proximity of the dates between the image acquisition and field data collection. The same set of VIs (Table 3) was derived using the extracted MODIS pixel values for individual biophysical characteristic model calibration. Since MODIS 250 m has the red and NIR bands only, indices such as VARI and $CI_{green}$ could not be derived at this resolution. For a pixel containing multiple sampling locations, the average value of the individual biophysical characteristic was calculated and used in model calibration. MODIS pixels corresponding to sampling locations which were too close to open water showed greater or similar observed NIR absorption compared to visible and had to be rejected from both the calibration and validation datasets. These pixels clearly contained a greater signal from water than vegetation and were considered water dominated mixed pixels. Further, due to occasional equipment failure such as sensor saturation, internal errors, and battery drain-out during field sampling, biophysical data from few study plots were either unavailable, or not usable for analysis. Post elimination of unusable pixels and ground data, model calibration was performed using 2010 field data and validation using 2011 field data. During this process, roughly 69 sampling plots established in 2010 were reduced to 10–15 usable MODIS 250 m and 7–10 usable MODIS 500 m pixels. For model validation, data set acquired during the field campaigns in 2011 containing 91 sampling plots were reduced to 10–12 MODIS 250 m pixels and 9–10 MODIS 500 m pixels. These were the reasons for the observed range of usable MODIS pixels for calibration and validation. Performance uncertainties were analyzed based on percent normalized root mean squared error (percent NRMSE) (Mishra et al., 2012), and residuals (observed–predicted). Percent NRMSE is estimated as:

$$\text{percent NRMSE} = \frac{RMSE}{(MAX\ (VALIDATION\ data) - (MIN\ (VALIDATION\ data))} \times 100. \quad (5)$$

### 4.3. Time-series composites and phenology characterization

Following successful calibration and validation, 8-day time-series composites were generated using ERDAS Imagine 2013 (ERDAS Imagine, Intergraph Corporation Part of Hexagon, Norcross, GA) for each biophysical characteristic (GLAI, VF, CHL, and GBM) from 2000 to

**Table 7**
Linear $R^2$ for MODIS (500 m) derived VIs calibrated against different biophysical characteristics. Most of the VIs (especially NIR based indices) show very poor/weak relationship with biophysical characteristics except for green–red based VARI. However, selection of best-fit model was done by examining the %NRMSE (Table 7) and residual trends.

| $R^2$ | NDVI | EVI2 | $CI_{red}$ | WDRVI ($\alpha = 0.1$) | WDRVI ($\alpha = 0.2$) | SAVI | GNDVI | $CI_{green}$ | VARI |
|---|---|---|---|---|---|---|---|---|---|
| GLAI | 0.097 | 0.128 | 0.214 | 0.184 | 0.159 | 0.097 | 0.004 | 0.000 | 0.910 |
| VF (%) | 0.165 | 0.192 | 0.236 | 0.249 | 0.227 | 0.165 | 0.006 | 0.000 | 0.980 |
| GBM ($gm^{-2}$) | 0.477 | 0.548 | 0.658 | 0.632 | 0.615 | 0.478 | 0.212 | 0.206 | 0.938 |
| CHL ($mgm^{-2}$) | 0.000 | 0.000 | 0.000 | 0.446 | 0.482 | 0.000 | 0.718 | 0.000 | 0.864 |

**Table 8**
Linear %NRMSE values for MODIS (500 m) derived biophysical models for different biophysical characteristics. %NRMSE of VARI was the lowest among the VIs tested; corroborating the failure of NIR based indices in terms of mapping biophysical characteristics coarser resolution.

| %NRMSE | NDVI | EVI2 | $CI_{red}$ | WDRVI ($\alpha = 0.1$) | WDRVI ($\alpha = 0.2$) | SAVI | GNDVI | $CI_{green}$ | VARI |
|---|---|---|---|---|---|---|---|---|---|
| GLAI | 41.567 | 42.447 | 44.205 | 43.578 | 43.115 | 41.570 | 40.015 | 38.436 | 32.474 |
| VF (%) | 55.175 | 54.103 | 49.832 | 51.803 | 52.900 | 52.946 | 41.988 | 41.175 | 24.344 |
| CHL ($mgm^{-2}$) | 93.594 | 84.891 | 70.034 | 75.027 | 78.890 | 93.569 | 84.946 | 67.190 | 21.998 |
| GBM ($gm^{-2}$) | 84.850 | 75.253 | 59.066 | 64.532 | 68.718 | 84.818 | 68.707 | 49.218 | 17.340 |

2014 using the best fit models. Map composites were generated for both 250 m and 500 m data. For each month, three to four composites per characteristic were created. Therefore, for an entire year, almost 46 composites were obtained for each biophysical characteristic. Composites were generated for all four characteristics, for the period 2000–2014. This amounted to more than 5500 8-day composites using both MODIS 250 m and 500 m data. These composites were then used for qualitative assessments of northern GoM tidal wetland condition before and after significant natural and anthropogenic events such as hurricanes and droughts over the period of 2000–2014.

Phenology charts for site specific tidal wetland patches were derived from these time-series composites, using spatial analysis module in ArcGIS (ArcGIS 10, Environmental Systems Research Institute, Redlands, California) for the growing seasons over the course of fifteen years. The sites for phenology characterization were chosen based on records of natural/anthropogenic events that have occurred and affected salt marsh habitats in the Northern Gulf coast. Here, we show the phenology derived for Terrebonne parish and Plaquemines parish of Louisiana, using MODIS 250 m and 500 m data respectively. We sampled 40 pixels from Terrebonne parish and 16 pixels from Plaquemines parish in order to extract biophysical values for deriving phenology. Monthly biophysical values were estimated using the average of all available 8-day composites within the month. The averaging was done to avoid the noise related to tidal fluctuations or modeling error propagated through the numerous processing steps involved in the phenology extraction. The phenology charts were developed to examine the impact of discrete natural and anthropogenic events on the health of specific salt marsh areas, as well as the overall long term trends in the tidal wetland health in the Gulf Coast.

## 5. Results and discussion

### 5.1. Tidal wetland reflectance properties

*In situ* spectral reflectance measured from most of the study plots of tidal wetland vegetation showed presence of reduced red-edge (Fig. 4a). The spectral reflectance derived from MODIS 500 m surface reflectance images showed a very similar overall trend (Fig. 4b). A

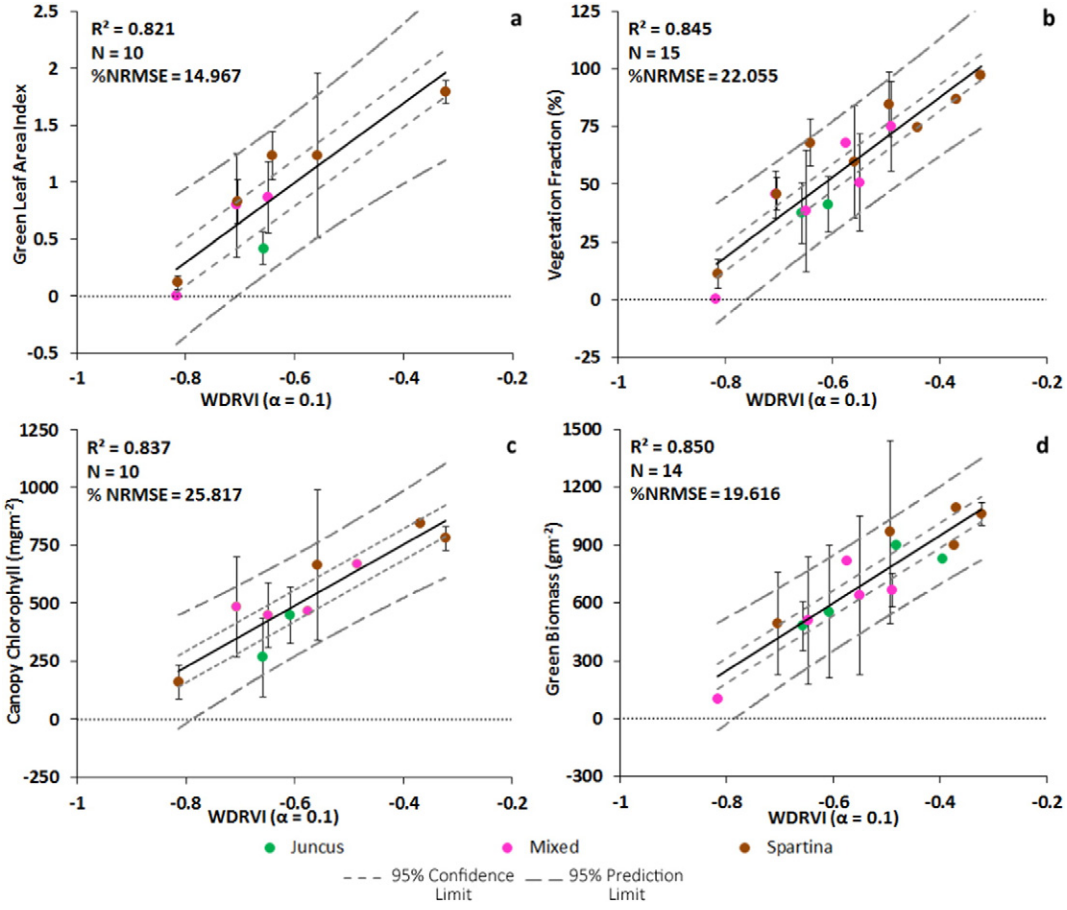


**Fig. 6.** Calibration of MODIS (250 m) derived WDRVI with a: GLAI, b: VF, c: CHL and d: GBM, with co-efficient of determination and 95% confidence intervals and limits. Error bars represent standard deviations. Coefficient of determination ($R^2$), sample size (N) and Percent Normalized Root Mean Square Error (%NRMSE) for respective models are also shown. Points with no error bars represent highly homogenous pixels with single study plots.

reduced red-edge does not necessarily mean that the vegetation is unhealthy; rather, it may be influenced by canopy structure, vegetation density, and NIR attenuation caused by signals from targets other than the vegetation itself. In case of tidal wetlands the reduced red-edge is understandable since these habitats are perennially inundated by tidal waters; even when the tides are low, significant residual moisture saturates the soil. Water and vegetation have contrasting spectral response in the NIR region of the spectrum; while vegetation has a tendency to scatter, water absorbs radiation in NIR. Therefore, the contrasting responses result in the presence of a reduced red-edge unlike terrestrial vegetation.

Further, variations in the spectral characteristics are also notable at the species level. *Spartina* and *Distichlis* on one hand have similar foliar and canopy structures much like flat-leaf grasses. *Juncus* and *Salicornia*, on the other hand have very unique foliar and canopy characteristics usually characterized by low chlorophyll and denser canopy structures with an overall low reflectance in the visible-NIR region of the spectrum, as measured from *in situ* spectral acquisition (Fig. 4c). Similar patterns were observed when the *in situ* ρ was averaged to MODIS visible and NIR bandwidths; the differences in the spectral response among different species were very much evident (Fig. 4d). Studying species level spectral response is crucial before biophysical model construction as it provides some pre-insight into potential performances of species specific or species independent models. As the species level spectral response showed significant differences, constructing species specific biophysical models seemed logical.

### 5.2. In situ reflectance based biophysical models

Three models were devise/developed using *in situ* hyperspectral spectra to estimate biophysical characteristics of (1) *Spartina*, (2) *Juncus*, and (3) mixed/all species combined dataset. Coefficient of determination ($R^2$) of the models of biophysical characteristics across species showed high variability and somewhat contrasting behavior (Fig. 5). For GBM, both linear and nonlinear models performed poorly in terms of explaining the total variation in the data, not only at the individual species level but also when data for all species were combined. VF variation was explained in *Spartina* by both linear and non-linear models. The VIs based on red and NIR bands performed relatively better than the indices based only on the visible bands such as VARI. The opposite was true for VF models of *Juncus* and all species combined, where VARI performed better than the red-NIR based VIs. Variation was reasonably explained by some linear and non-linear models for $CHL_c$ in *Juncus*, whereas, few non-linear quadratic models reasonably explained good variation in *Spartina*. The model performances dropped considerably when all species were combined. Similar trends were observed for GLAI, which is expected since $CHL_c$ is derived as a function of LAI. In general, the performances of VIs were not only inconsistent across species but also across different biophysical characteristics.

In addition, Pearson's rank correlation test showed significant correlations between almost all VIs and GBM (both in *Spartina* and *Juncus*) and VF (only in *Juncus*) at the 0.05 level of significance. CHL, VF, and GLAI did not bear significant correlations with VIs in *Spartina*. No significant correlation was observed between VIs and biophysical

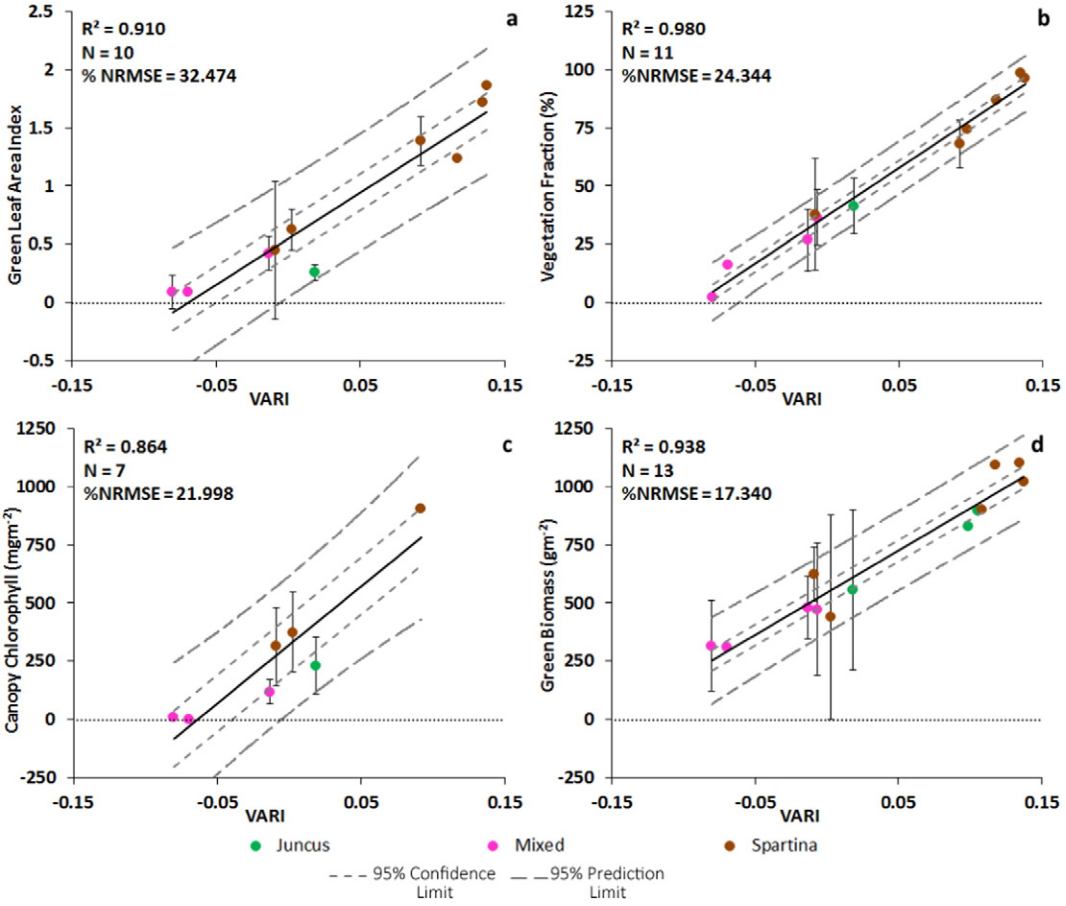


**Fig. 7.** Calibration of MODIS (500 m) derived VARI with a: GLAI, b: VF, c: CHL and d: GBM, with co-efficient of determination and 95% confidence intervals and limits. Error bars represent standard deviations. Coefficient of determination ($R^2$), Sample size (N) and Percent Normalized Root Mean Square Error (%NRMSE) for respective models are also shown. Points with no error bars represent highly homogenous pixels with single study plots.

characteristics when all homogenous plots were combined (Table 4). The heterogeneous plots also did not exhibit strong relationships between *in situ* VIs and biophysical characteristics. The initial calibration attempted with Ocean Optics hyperspectral data was not encouraging enough to develop models to be tested for validation with MODIS data. The lack of satisfactory performance in model calibration when using *in situ* hyperspectral data is attributed mainly to the strong influence of species variability. *In situ* reflectance spectra, particularly in NIR show significant variability across species because of the variations in cell structure and canopy architecture. That variability is somewhat lost in MODIS data because of the averaging effect over a broad area (Fig. 4a–d).

### 5.3. MODIS based biophysical models

After an extensive testing of numerous VIs retrieved from MODIS data using the aforementioned calibration and validation methods, the WDRVI ($\alpha = 0.1$) (Gitelson, 2004) was selected for estimating the biophysical characteristics (GLAI, CHL, VF, GBM) for the 250 m data, whereas, VARI (Gitelson et al., 2002b, 2002a) was selected for estimating the biophysical characteristics for the 500 m data (Tables 5–8; Figs. 6–7). The performances of the non-linear models were similar to that of the linear ones in terms of $R^2$ and %NRMSE. Therefore, to avoid the saturation tendencies of non-linear models either at the very low or very high values, linear best fit models were used for both 250 m and 500 m data. Further, it was observed that the performances of several red-NIR based VIs on 250 m data were similar to each other (Tables 5 and 6; Fig. 6). This might be due to the fact that almost all of these VIs tend to normalize the differences between NIR and red bands, using different coefficients, to increase their sensitivity across a broad range of biophysical characteristics. Therefore, their overall performances in estimating biophysical characteristics will be very comparable, especially for a relatively low aboveground biomass ecosystem such as wetlands. For 250 m data, the few models that showed the highest $R^2$ such as NDVI, EVI2, and SAVI also showed high %NRMSE during validation. This may be due to some inherent bias in the models or a lack of uniform sensitivity for the entire range of biophysical characteristics. To further investigate the overlapping performance of the VIs, we examined the residual (measured–predicted) and the slope ratio ($M_v/M_c$), ratio of the slopes of the validation ($M_v$) and calibration ($M_c$) trend-line, for all models. $M_v/M_c$ should be close to 1 for models with minimum bias and maximum sensitivity across the entire range of biophysical characteristics. Selecting

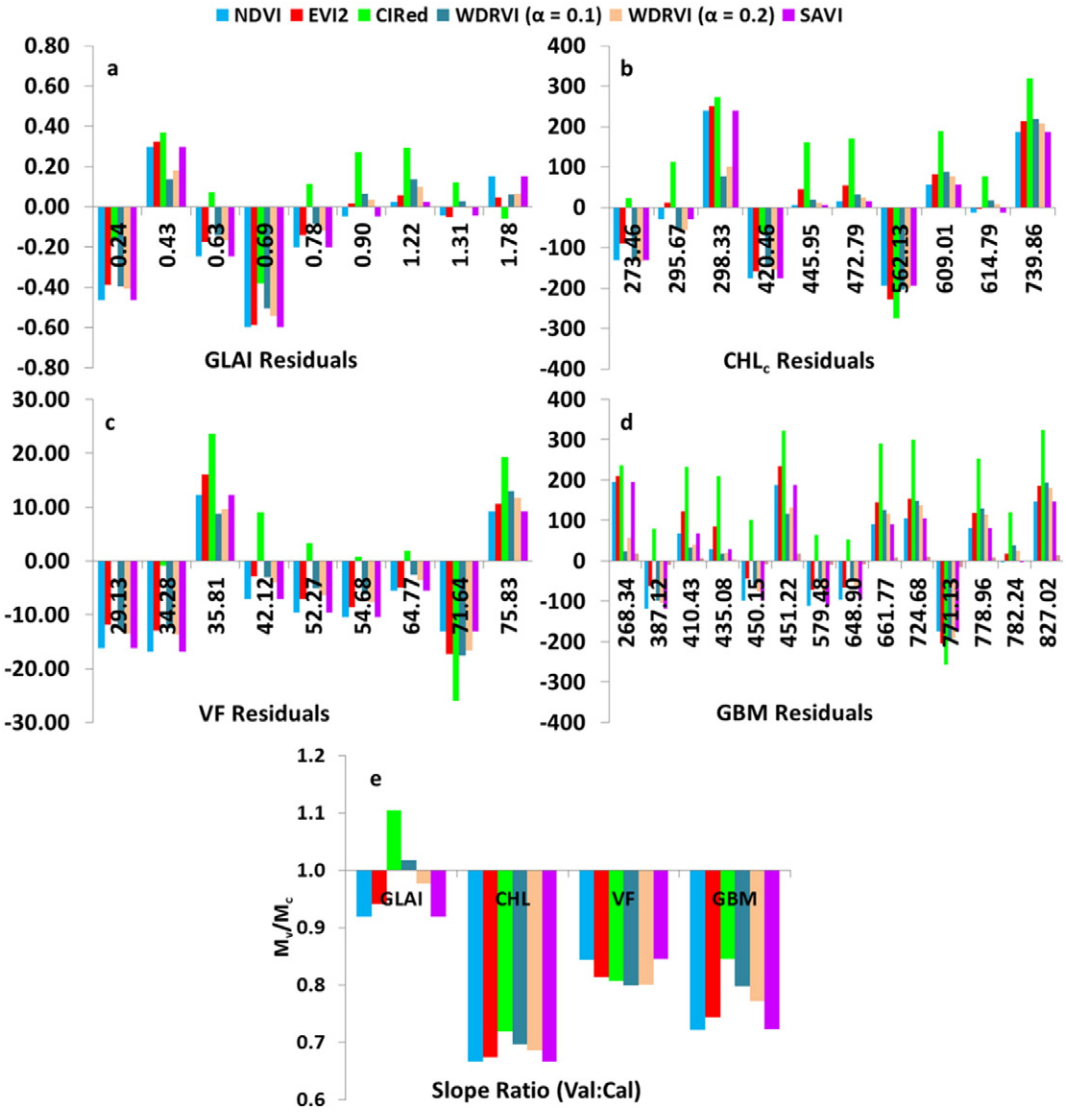


**Fig. 8.** Residual plots for MODIS (250 m) based biophysical models for a: GLAI, b: CHL, c: VF and d: GBM. WDRVI ($\alpha = 0.1$) was chosen as the best-fit model. e: Slope ratio between linear trends of validation and calibration data. Models with minimum bias have ratios close to 1.

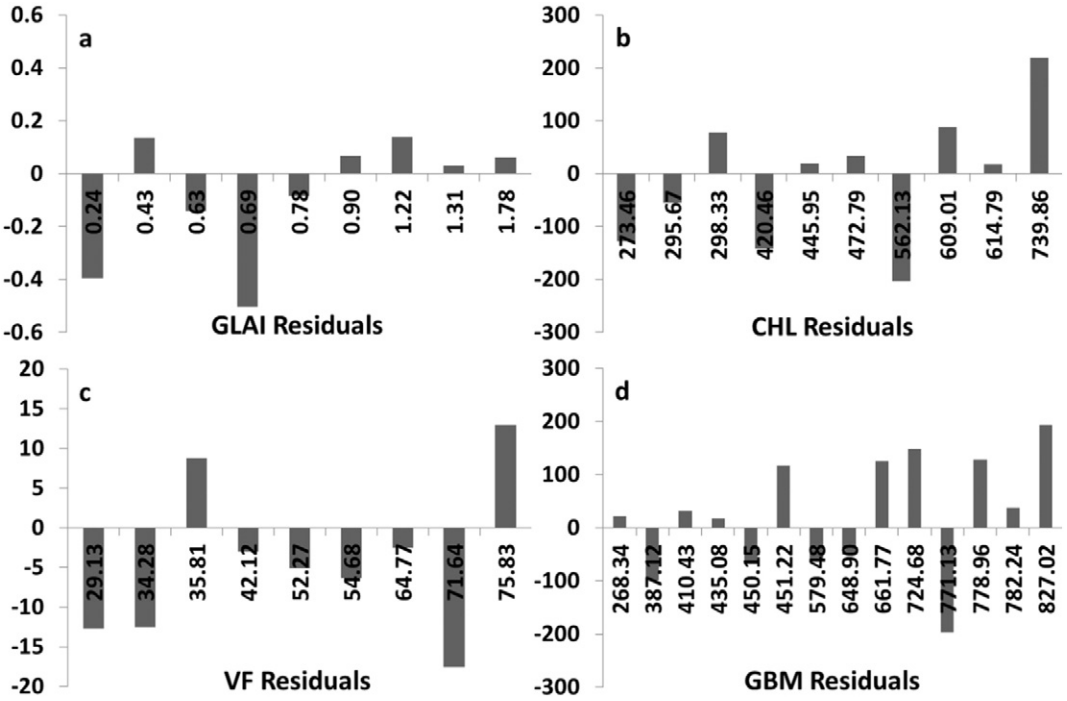


**Fig. 9.** Residual plots for MODIS (500 m) based best fit biophysical models (using VARI) for a: GLAI, b: CHL, c: VF and d: GBM.

the best model for MODIS 250 m data, therefore, was not straightforward. In order to choose the best model for all biophysical characteristics, we had to methodically eliminate all of the other models. This was done considering a combination of factors such as $R^2$, %NRMSE, $M_v/M_c$, and residual trends (Tables 5 and 6; Fig. 8a–e). First, we eliminated three models, NDVI, EVI2, and SAVI, which showed relatively high %NRMSE (Table 6) but highest deviation of $M_v/M_c$ (Fig. 8e). The highest deviation of $M_v/M_c$ for the three VIs also explained their lack of uniform sensitivity across the entire range of biophysical characteristics and high RMSE in their predictions. This is further evident in residual trends which indicated that NDVI, EVI2, and SAVI produced some of the highest errors at the very low and very high magnitude of each biophysical characteristic (Fig. 8a–d). Next, we discarded $CI_{red}$, which showed an overall trend of under-estimation in residual plots (Fig. 8a–d). Finally, we eliminated WDRVI ($\alpha = 0.2$) which showed marginally higher deviation in slope ratio compared to ($\alpha = 0.1$). As such, WDRVI ($\alpha = 0.1$) was selected as the best fit model and was used to model and map the biophysical characteristics using MODIS 250 m data. The WDRVI based linear models developed for mapping biophysical characteristics are as follows:

$$GLAI = 3.4886 \times WDRVI\ (\propto = 0.1) + 3.0865 \quad (6)$$

$$CHL = 1328.3 \times WDRVI\ (\propto = 0.1) + 1285.036 \quad (7)$$

$$VF = 172.74 \times WDRVI\ (\propto = 0.1) + 156.75 \quad (8)$$

$$GBM = 1757.423 \times WDRVI\ (\propto = 0.1) + 1654.197. \quad (9)$$

For 500 m data, however, it was observed that VARI outperformed all other VIs by a large margin (Tables 7 and 8; Figs. 7 and 9). The overlapping performances of the VIs encountered in 250 m data were not present in 500 m data. This might be due to the enhanced water signal and increasingly fragmented patches of wetlands, at the coarser 500 m resolution making the NIR band unresponsive for vegetation specific analyses, particularly for the red-NIR based VIs. It is relatively difficult to find homogenous wetland pixels in 500 m data compared to 250 m

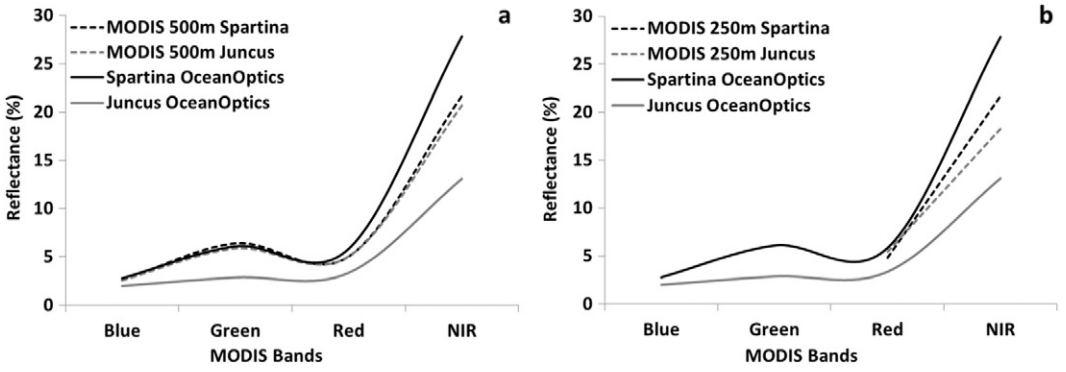


**Fig. 10.** Comparison between reflectance (%) between Ocean Optics and MODIS derived spectral response for *Spartina* and *Juncus* from a: 250 m and b: 500 m spatial resolution. The plots show how species information is lost with progressive decrease in spatial resolution. MODIS 250 m dataset does not have blue and green bands; as such spectral information for those bands are missing in Fig 10a.

data without having high influence of water background because tidal wetlands are by nature fragmented and heavily interspersed with creeks and channels. Therefore, despite careful study site and pixel selection before and during field visits, as well as in subsequent analysis, presence of enhanced water signal in the 500 m data becomes unavoidable. This could be the reason why a green–red based VI such as VARI showed the highest sensitivity to the wetlands biophysical characteristics. As evident for Tables 7 and 8, VARI outperformed other VIs in terms of explaining the variance in the field data used in the model, as well as prediction errors. The linear models used for mapping biophysical characteristics for 500 m are as follows:

$$GLAI = 7.8917 \times VARI + 0.5532 \quad (10)$$

$$CHL = 5041.7 \times VARI + 321.16 \quad (11)$$

$$VF = 409.42 \times VARI + 37.571 \quad (12)$$

$$GBM = 3617.104 \times VARI + 543.3514. \quad (13)$$

### 5.4. Performance comparison: MODIS vs in situ

From the calibration results, it was clearly evident that MODIS based biophysical models outperformed models derived from Ocean Optics based *in situ* hyperspectral data integrated to represent MODIS bands. This was counterintuitive and interesting, because Ocean Optics data were acquired almost at a controlled setting over a homogenous sub-plot, in contrast to MODIS data where the degree of homogeneity was hard to maintain. Therefore, it was expected that the Ocean Optics data would be a better representative of the vegetation's biophysical characteristics. Our results indicated otherwise. In order to investigate the reason behind this, we compared spectral reflectance patterns of the dominant species *Spartina* and *Juncus* derived from both Ocean Optics and the MODIS sensor. Results demonstrate strong variability between *Spartina* and *Juncus* at the ground level (Schmidt & Skidmore, 2003), when spectral profiles are acquired by the Ocean Optics hyperspectral sensors. However, species level spectral variability seem to become diluted as the scale of the study site becomes coarser, as observed in the MODIS derived spectral response for both 250 and 500 m data (Fig. 10). This clarifies the contrasting performances between the

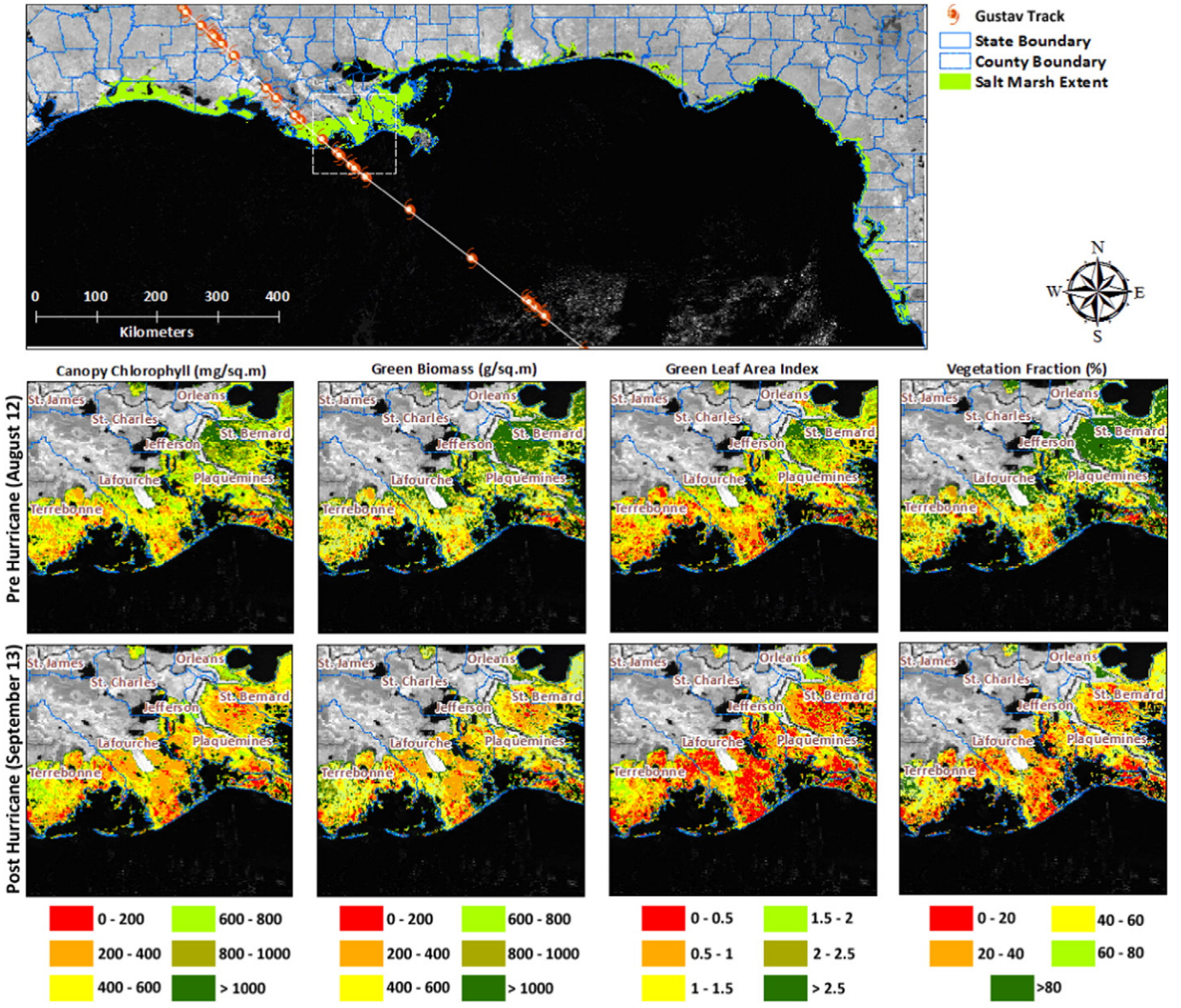


**Fig. 11.** Sample composites (top image) showing spatial distribution of biophysical characteristics (in this case GBM) for four Gulf States using MODIS 250-m data. Expanded maps showing the magnitude and distribution of CHL, GBM, GLAI, and VF pre-and post-Hurricane Gustav.

MODIS derived and Ocean Optics derived VIs. Variation in the spectral response at the ground level can be explained by the foliar and canopy structures of *Spartina* and *Juncus*. Low average chlorophyll content and canopy structure of *Juncus* are also responsible for the absence of considerable scattering in the NIR band. *Spartina*, with relatively high chlorophyll content and canopy structure characterized by broader leaf area scatters more radiation in the NIR region. NIR reflectance is primarily controlled by leaf structure and canopy architecture; since *Spartina* and *Juncus* have very different leaf structure, the spectral variability for the two species in NIR is also the highest (Fig. 10). However, as the scale becomes coarser, i.e. at the MODIS satellite level, the species specific spectral variability is lost, and therefore, at the landscape level, species invariant models based on MODIS seem to perform better than models based on *in situ* ρ.

Further, as is evident from model performances, for both 250 m and 500 m resolutions, red-NIR band based VIs performed reasonably well; however, VIs based on only visible bands using MODIS 500 m datasets had better correlations with the biophysical characteristics. This can also be explained by the loss of species specific signal in coarse resolution data, where a high degree of similarity is noticed in the spectral response of species in the visible and NIR region of the spectrum (Fig. 10). This might also be attributed to the complex nature of tidal wetland habitats, where homogenous patches are often interlaced by tidal creeks and channels, fed by the tidal waters. Water signals from those channels, as well as from the surrounding rivers/ocean, are highly influential in minimizing the reflectance in the NIR region, making it insensitive to species variability, with progressive coarseness in the spatial resolution. Tidal stage at the time of MODIS image acquisition also has a significant effect on the biophysical models, as images acquired during high tides considerably affect the sensitivity of the NIR, and subsequently reduce the sensitivity of red and NIR based vegetation indices. When using MODIS daily surface reflectance data, it is certainly possible to develop a filter to flag the tide dominated scenes by matching tide level from the nearby tide gauge(s) with the MODIS overpass time. However, since we are utilizing the MODIS 8-day surface reflectance products, which provide us with pre-calculated average reflectance over 8-day time period, it is not possible to determine the level of daily MODIS scene contribution to the 8-day surface reflectance imagery. In other words, it is not possible to determine for a particular pixel, whether it is an average of the complete 8 days of surface

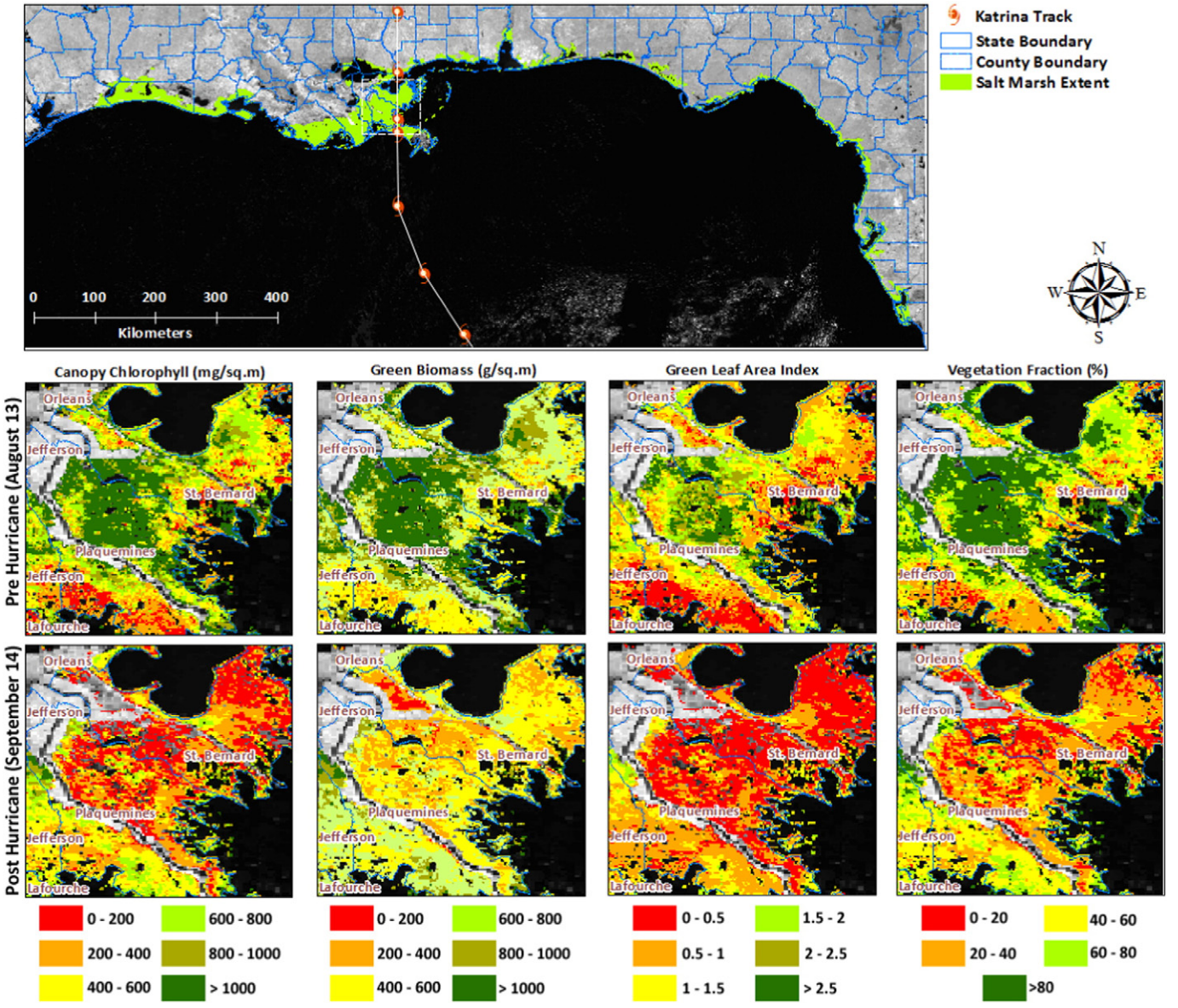


**Fig. 12.** Sample composites (top image) showing spatial distribution of biophysical characteristics (in this case GBM) for four Gulf States using MODIS 500-m data. Expanded maps showing the magnitude and distribution of CHL, GBM, GLAI, and VF pre-and post-Hurricane Katrina.

reflectance, or less than that. Therefore, tidal influence could be one source of variability in the biophysical models.

### 5.5. Time-series composites and phenological analysis

The time-series map composites that we generated for the 15 year time period using the best fit models for both 250 m and 500 m data provide relevant qualitative assessment of the biophysical status of the tidal wetlands (Figs. 11 and 12). In particular, the models were able to illustrate the effects of large scale natural disasters affecting the region. For example, a comparison between the time-series composites pre and post hurricane Gustav, using MODIS 250 m datasets, clearly illustrates the impact of the landfall, in southern LA. Gustav made landfall at Terrebonne Parish on September 1st, as a Category-2 hurricane, and downgraded to a tropical storm hours later causing heavy rainfall and flooding in Plaquemines, Jefferson, and St. Bernard Parish (~ 25-40 cm. rainfall between August 29 and September 5; http://www.weather.gov). The 8-day composite derived from the MODIS image of August 5, 2008 showed high levels of CHL, GBM, GLAI and VF for those regions which is expected during the middle of the growing season. Post hurricane composites showed significant reduction in the levels of all biophysical characteristics, indicating severe short-term physical impact of the high energy phenomenon on the tidal wetland habitats (Fig. 11). Over the years hurricanes have severely impacted the Gulf Coast wetlands by causing substantial short-term damage due to a combination of wind, tide, and wave action. Most of the physical damage due to hurricane landfall includes (a) compressed marsh – a net decrease in surface area resulting from marsh being pushed together, (b) marsh balls – marsh being piled, rolled, and deformed to create large mounds, and (c) sediment deposition on marsh grass (Lovelace & McPherson, 1998). The biophysical map composites before and after Gustav demonstrated this immediate physical damage (Fig. 11). Comparison between MODIS based GBM estimates from Terrebonne Parish with the monthly GBM estimates reported by Darby and Turner (2008) from a tidal wetland patch in approximately the same geographic area (accurate GPS location of their study area was unavailable) reveal some differences between GBM magnitude and phenology, particularly at the peak of the growing season. The peak biomass estimates from MODIS 250 m data (634.7 $gm^{-2}$; October 2004) were less than their plot level estimates (877 $gm^{-2}$; September, 2004). Further, MODIS based model predicted the peak biomass level in October rather than in September as reported in their study. Similar differences were also noticed at the beginning of growing season. MODIS estimates of biomass from March 2004 (402.3 $gm^{-2}$) were being much higher than 114 $gm^{-2}$ as observed by Darby and Turner (2008). Differences in the estimates could be due to the difference in location of the exact sites or due to mismatch between plot level estimates (their study) and coarse pixel level estimates (our study).

A similar comparison between pre and post Hurricane Katrina is shown using time-series composites generated from MODIS 500 m datasets. Katrina made its second landfall in the Plaquemines parish as a Category 3 hurricane and maintained its intensity as it passed over St. Bernard parish towards New Orleans (Waple, 2005). The reduction in the levels of biophysical characteristics indicated severe stress in the tidal wetland habitats in the Plaquemines, Jefferson and St. Bernard Parish near New Orleans (Fig 12). From these examples it is quite clear that such high frequency time-series map composites can not only help to identify extent and magnitude of physical damage to wetland patches after similar natural or anthropogenic disasters, but can also facilitate restoration and conservation measures. The high temporal resolution of the MODIS products allows for frequent monitoring, leading to rapid initiation of restoration efforts after disturbances and accurate monitoring of the restored habitats.

In addition, phenological charts derived from the time-series composites illustrate the trends in the biophysical values quantitatively (Figs. 13 and 14). The MODIS based biophysical models enabled us to develop 15 years of high frequency phenology for any wetland site across the four Gulf States. The site specific phenology shown in this study for selected locations in Terrebonne and Plaquemines parishes have been able to capture not only the natural seasonal variability, but

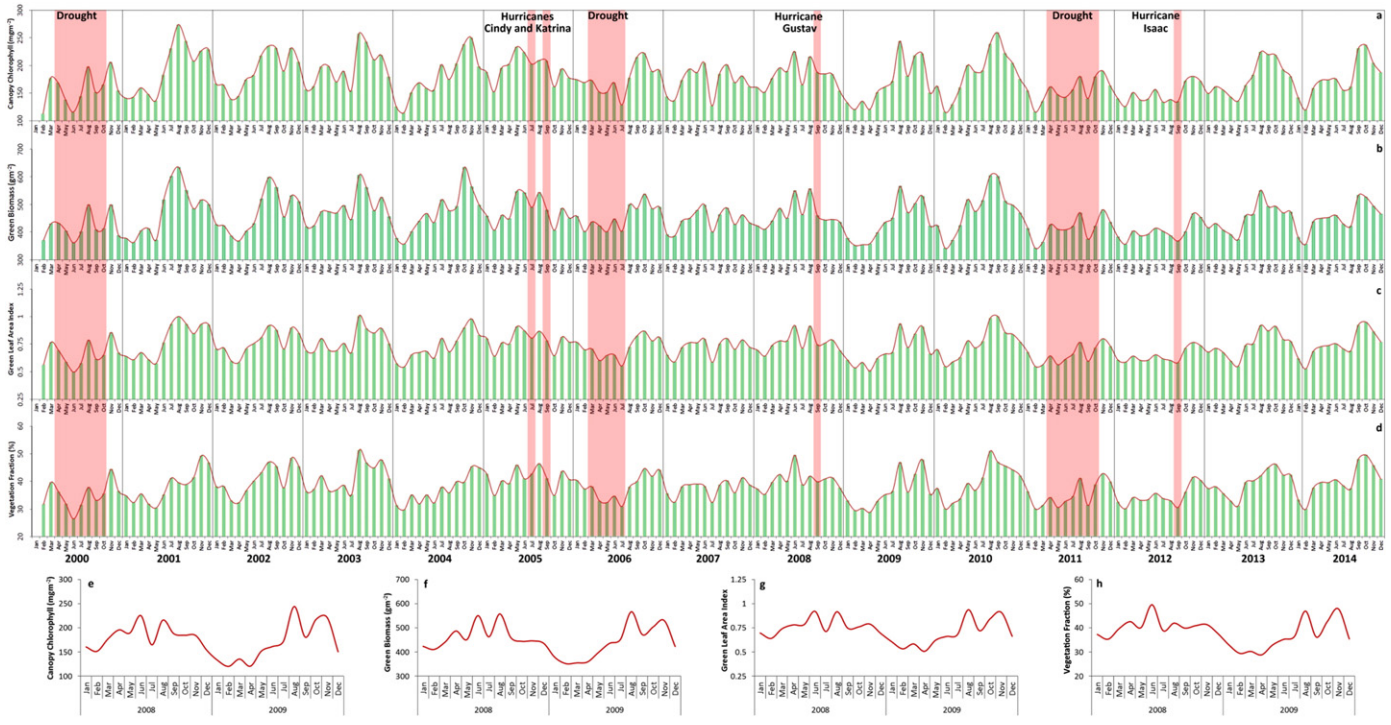


**Fig. 13.** Phenological variations in a: CHL, b: GBM, c: GLAI, d: VF in tidal wetlands of Terrebonne Parish, LA, from 2000 to 2010 (250 m MODIS data). The effects of Hurricanes Cindy, Katrina, Gustav, and Isaac and periodic Droughts have been highlighted. Comparisons between the levels of e: CHL, f: GBM, g: GLAI and h: VF in the growing seasons of 2008 and 2009 has been shown as specific example.

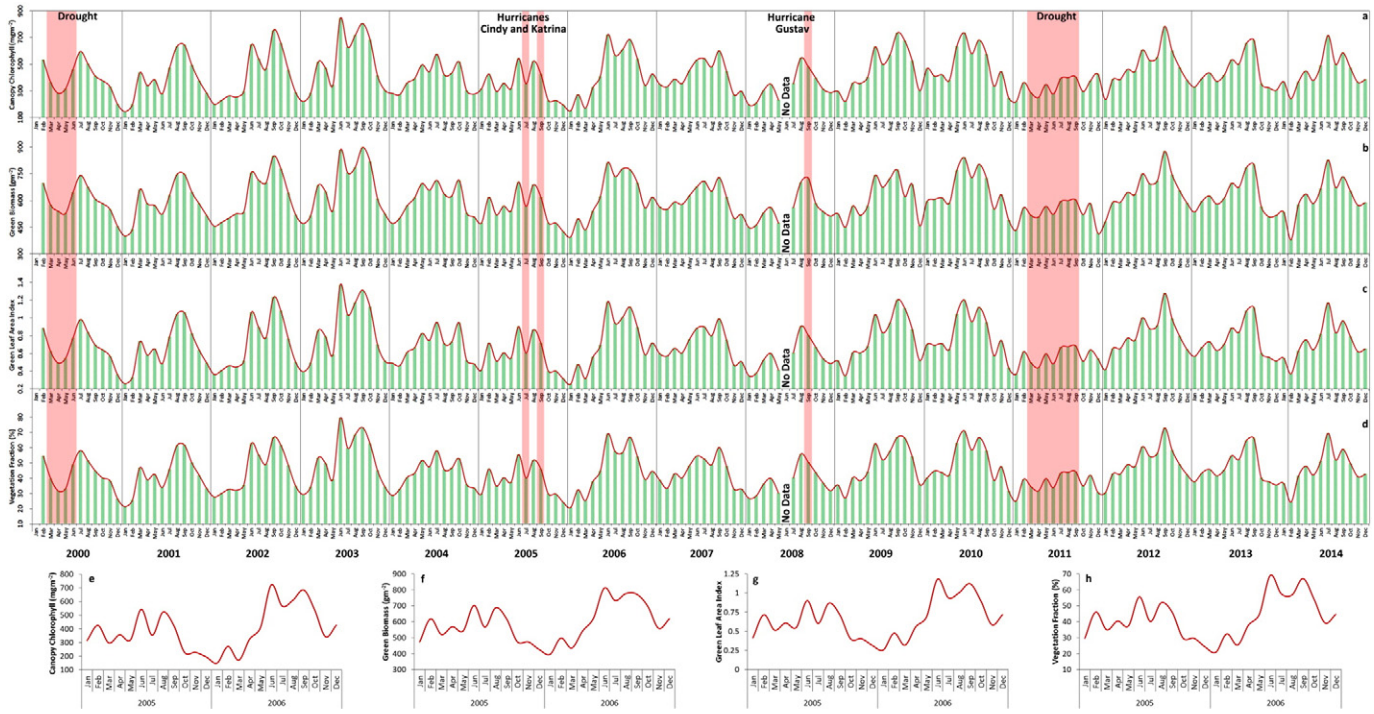


**Fig. 14.** Phenological variations in a: CHL, b: GBM, c: GLAI, d: VF in tidal wetlands of Plaquemines Parish, LA, from 2000 to 2010 (500 m MODIS data). The effects of Hurricanes Cindy and Katrina, and Gustav, and periodic Droughts have been highlighted. Comparisons between the levels of e: CHL, f: GBM, g: GLAI and h: VF in the growing seasons of 2005 and 2006 has been shown as specific example.

also the effects of various natural and anthropogenic events that have occurred between 2000 and 2014 on the wetland biophysical status. These sites were carefully chosen for analysis, as they are not only diverse in terms of species composition, but also they have been subject to episodic tropical storms and severe drought, which have induced stress on the tidal wetland habitats. Therefore, these sites can be considered as periodic critical hotspots of tidal wetland stress and degradation.

The growing season of tidal wetlands along the Gulf Coast usually begins in March/April and reaches peak growth and photosynthetic activity in August/September, followed by period of senescence and dormancy from October until the beginning of the next growing season. Natural or anthropogenic disasters induce both short and long-term stress in these wetland habitats. Hurricanes and similar high energy phenomena such as tropical storms have been known to cause moderate to severe short-term physical damage to wetlands. For example, the short-term effects of hurricanes Cindy and Katrina (2005), Gustav (2008) and Isaac (2012) on the wetlands in Terrebonne parish are visible by the obvious reduction in the magnitudes of biophysical characteristics after each event shown in both the MODIS 250 m composites and phenology plot (Fig. 13). Further, stress induced by periodic drought are also visible in the growing seasons of 2000, 2006, and 2011, when wetlands witnessed extreme (D3) to exceptional (D4) dry conditions in LA (US drought monitor archives; http://droughtmonitor.unl.edu/) (Fig. 13a–d). A closer examination of the growing seasons of 2008 and 2009 clearly shows the stress induced by Hurricane Gustav in September 2008 similar to the effects seen in the map composites (Fig. 11). However, the steady recovery from the stress is also visible in the 2009 phenology when the wetland habitats returned to the pre-hurricane biophysical levels by August 2009 (Fig. 13e–h). It demonstrates the resiliency of these wetlands even in the face of high intensity hurricanes. Möller et al. (2014) showed that up to 60% of observed wave attenuation can be attributed to marsh vegetation. They also found that although storm waves cause considerable physical damage to the stem and canopy of the vegetation, the marsh surface remains stable and resistant to surface erosion under all conditions. We found similar behavior in our phenology plots, which showed that Gulf wetlands suffered severe short-term damage but bounced back after every hurricane because their surface and belowground architecture remained stable. Similarly, the 500 m data derived phenology derived from wetland patches in Plaquemines parish, LA illustrates the impact of Hurricanes Cindy and Katrina in the growing seasons of 2005, and drought in 2000 and 2011. Comparative analysis between the growing seasons of 2005 and 2006 shows recovery of the wetland habitats from the stress induced by back-to-back landfall of Hurricanes Cindy and Katrina in the region (Fig. 14 e–h). The effects of the stress seem directly proportional to the intensity and duration of a natural or anthropogenic event (such as Hurricane strength or length of drought period). Further, the magnitude of the impact also depends on the timing of an event. Stress induced during the middle of the growing season, when photosynthesis, growth and reproduction rates are high and susceptible to any environmental disturbances, is much more pronounced compared to disturbances during the non-growing season, when wetland plants are already in a stage of senescence.

In addition to events captured through phenology analysis, other fluctuations were also seen in the seasonal trends of the biophysical values; these may have been a result of natural variability, localized disturbances, or model uncertainties. Although detailed site-specific phenological analysis of tidal wetland habitats is beyond the scope of this study, it is undeniable that such phenological plots have the potential to provide both quantitative estimates of site specific characteristics, and the long-term trend of the tidal wetland health. MODIS is the only existing sensor that provides 8-day cloud free products which are necessary for high frequency regional phenological analysis. Such long-term trends can also be analyzed in conjunction with long-term climate data, such as temperature and sea level rise, to assess and predict response of tidal wetlands climatic forcings.

MODIS derived time-series map composites and phenological charts provide coastal resource managers and policy makers with both qualitative and quantitative information of the status of tidal wetlands. The biophysical mapping methodology developed through this study can be used for identifying critical 'hotspots' of wetland degradation due to factors other than natural disasters such as developmental activities, oil and gas industry activities, urban runoff, sudden marsh die-off events, changes in soil biogeochemical properties, and herbivory. The models and products developed through this study have the potential to facilitate prioritization of restoration efforts through identification of areas in need of immediate attention; they can also be used to compare the biophysical status of wetland patches/habitats pre and post implementation of restoration.

## 6. Conclusion

This study provides novel methods for mapping tidal wetland health and productivity, using fine temporal resolution MODIS data. For the first time statistical models were established for wetland biophysical characteristics by combining MODIS derived VIs and extensive ground data. This kind of regional wetland study has not been previously attempted at such a large scale because of the inherent difficulty in collecting ground data to represent coarse resolution satellite pixels. Furthermore, ground data collection can be expensive and time consuming. The MODIS based models developed in this study have been able to map these biophysical characteristics effectively, and can serve as baseline for developing satellite based models of NPP/CSP potential of the tidal wetlands. Mapping NPP/CSP is crucial for detecting whether these ecosystems are functioning as sinks or sources of carbon in the environment. This is particularly important because these productive coastal ecosystems in the Gulf and elsewhere are vulnerable to climate change induced sea level rise and perpetual developmental pressures. Our approach to study tidal wetlands is different from conventional tidal remote sensing approaches which have concentrated on habitat delineation, species mapping and/or wetland gain/loss.

The biophysical characteristics, analyzed in this paper (GLAI, VF, $CHL_c$ and GBM) are suitable proxies for photosynthetic capacity, nitrogen content, and the physiological status (Blackburn, 1998; Pierce, Running, & Walker, 1994; Pinar & Curran, 1996) of wetland vegetation since they are sensitive to natural processes and anthropogenic activities occurring across the region. These biophysical characteristics can be different between species of wetland vegetation due to their differences in foliar and canopy structures, distribution, and habitat preference, and inherent physiology. Species-dependent wetland biophysical models are generally more accurate and can be implemented only when wetlands in the study area can be classified into individual plant communities. Classification of the wetland habitats into homogenous species communities is impractical as it requires significant ground data and tidal information; it is particularly difficult when using moderate and coarse spatial resolution sensors such as MODIS because of mixed pixel issues. Further, unavoidable classification errors can be introduced during mapping species composition prior to application of these biophysical models, which in turn have built-in uncertainties, which magnifies the error of the final output. As such, the information provided to the end user (restoration managers and conservationists) may be far from the reality. Therefore, using species-independent biophysical models (not influenced by species diversity), is the best option to generate high frequency time-series composites. Moreover, our analysis and results clearly demonstrate the deterioration of the species level signal variation at the coarse spatial resolution of MODIS, which makes it suitable for broad scale regional mapping. This study has demonstrated the value of species-invariant biophysical models, which can be implemented for any wetland habitat regardless of its community composition. In addition, since these MODIS based models are species independent, they can be utilized for monitoring similar tidal wetland habitats within United States such as coastal Georgia, Texas, California, and the Carolinas, as well as marshes in the temperate zones throughout the world. For other wetland habitats, such as the mangroves and freshwater wetlands, these biophysical models may be applied after recalibration and optimization. This is due to the fact that mangroves and freshwater wetlands have significantly different foliar and canopy architecture.

Although MODIS can be an excellent choice for broader landscape level biophysical mapping, certain site specific studies may require information at a much finer resolution. Mapping biophysical parameters using species specific models might be a better option than species invariant models if species classification map is available for a study site. Further, in order to implement these biophysical models using MODIS for a particular tidal wetland habitat the extent of the habitat has to be completely covered by at least 8–10 pixels of MODIS 250 m or 500 m, which may be impossible in highly fragmented habitats. In essence, selection of the appropriate sensor for biophysical mapping should depend not only on the research questions and scale, but also on the nature of the wetland habitat. Since the models are somewhat influenced by tidal fluctuations, developing tide invariant models should be the next step which is certainly feasible on temporally dense MODIS daily surface reflectance data.

The high temporal resolution of MODIS 8-day surface reflectance products, coupled with the moderate spatial resolution, has immense potential in studying and monitoring both long and short-term tidal wetland health and physiological status. Further studies can be performed both at site specific and landscape levels. The time-series maps and phenological charts derived from MODIS imagery provide the tools necessary for effective conservation and restoration of these fragile ecosystems. These products can be used in conjunction with different hydrological, meteorological, and land-use parameters to assess the influence of different factors on wetland health. Coastal resources managers and policy makers in the Gulf Coast will now have access to large-scale maps of the status of the wetlands under their jurisdiction and can use these products to (a) identify problem areas that should be high priorities for restoration activities, (b) evaluate the relative success of prior restoration efforts, and (c) locate the vulnerable wetland patches most likely to be affected by coastal developmental activities.

## Acknowledgments

This study involved intense field data collection spanning over three years under harsh conditions and we would like to thank and acknowledge the large number of people involved in this effort, including Chris Downs, Mike Bryant, Calista Guthrie, Gary Alon Blakeney and Sachidananda Mishra (Mississippi State University), Paul Merani (University of Nebraska–Lincoln), Philemon Kirui (Jackson State University), Sarah Moore, Ross Del Rio, Lindsay Dunaj, Phil McCarty, Mike Brown (University of New Orleans), Christina Mohrman (Grand Bay National Estuarine Research Reserve), and Charles Jordan (University of Georgia). This research was partially funded by the National Aeronautics and Space Administration (NASA) Gulf of Mexico program (Grant # NNX10AE65G), National Science Foundation (NSF) Division of Environmental Biology (Grant # 1050500), and Gulf of Mexico Research Initiative (GoMRI) (Grant # GRI-0012). Anatoly Gitelson is grateful to International Incoming Marie Curie Fellowship for supporting this work at Israel Institute of Technology.

## References

Adam, E., Mutanga, O., & Rugege, D. (2010). Multispectral and hyperspectral remote sensing for identification and mapping of wetland vegetation: a review. *Wetlands Ecology and Management, 18*, 281–296.

Artigas, F., & Pechmann, I. C. (2010). Balloon imagery verification of remotely sensed *Phragmites australis* expansion in an urban estuary of New Jersey, USA,. *Landscape and Urban Planning, 95*, 105–112.

Baldocchi, D. D. (2003). Assessing the eddy covariance technique for evaluating carbon dioxide exchange rates of ecosystems: past, present and future. *Global Change Biology, 9*, 479–492.

Barbier, E. B., Koch, E. W., Silliman, B. R., Hacker, S. D., Wolanski, E., Primavera, J., Granek, E. F., Polasky, S., Aswani, S., Cramer, L. A., Stoms, D. M., Kennedy, C. J., Bael, D., Kappel, C. V., Perillo, G. M. E., & Reed, D. J. (2008). Coastal ecosystem-based management with nonlinear ecological functions and values. *Science*, *319*, 321–323.

Bertness, M. D., Silliman, B. R., & Holdredge, C. (2009). Shoreline development and the future of New England salt marsh landscapes. In B. R. Silliman, E. D. Grosholz, & M. D. Bertness (Eds.), *Human Impacts on Salt Marshes: A global perspective* (pp. 137–148). California, USA: University of California Press, Berkeley.

Biber, P. D. (2007). Evaluating a chlorophyll content meter on three coastal wetland plant species. *Journal of Agriculture, Food and Environmental Science*, *1*, 1–11.

Biber, P. D., Wu, W., Peterson, M. S., Liu, Z., & Pham, L. (2012). *Oil contamination in Mississippi saltmarsh habitats and the impacts to Spartina alterniflora photosynthesis, in: Impacts of oil spill disasters on marine habitats and fisheries in North America (in press)*. Boca Raton, Florida, USA: CRC Press.

Blackburn, G. A. (1998). Quantifying chlorophyll and carotenoids at leaf and canopy scales: An evaluation of some hyperspectral approaches. *Remote Sensing of Environment*, *66*, 273–285.

Boesch, D. F., & Turner, R. E. (1984). Dependence of fishery species on salt marshes: The role of food and refuge. *Estuaries*, *7*, 460–468.

Brevik, E. C., & Homburg, J. A. (2004). A 5000 year record of carbon sequestration from a coastal lagoon and wetland complex, Southern California, USA. *Catena*, *57*, 221–232.

Campbell, J. B. (Ed.). (2007). *Introduction to remote sensing, Guilford, New York*. New York: USA.

Chmura, G. L., Anisfeld, S. C., Cahoon, D. R., & Lynch, J. C. (2003). Global carbon sequestration in tidal, saline wetland soils. *Global Biogeochemical Cycles*, *17*. http://dx.doi.org/10.1029/2002GB001917.

Choi, Y., & Wang, Y. (2004). Dynamics of carbon sequestration in a coastal wetland using radiocarbon measurements. *Global Biogeochemical Cycles*, *18*. http://dx.doi.org/10.1029/2004GB002261.

Churkina, G., Schimel, D., Braswell, B. H., & Xiao, X. M. (2005). Spatial analysis of growing season length control over net ecosystem exchange. *Global Change Biology*, *11*, 1777–1787.

Collin, A., Long, B., & Archambault, P. (2010). Salt-marsh characterization, zonation assessment and mapping through a dual-wavelength LiDAR. *Remote Sensing of Environment*, *114*, 520–530.

Connor, R. F., Chmura, G. L., & Beecher, C. B. (2001). Carbon accumulation in Bay of Fundy salt marshes: Implications for restoration of reclaimed marshes. *Global Biogeochemical Cycles*, *15*, 943–954.

Dahl, T. E. (2006). *Status and trends of wetlands in the conterminous United States 1998 to 2004*. Washington D. C., USA: Fish and Wildlife Service, Fisheries and Habitat Conservation.

Darby, F. A., & Turner, R. E. (2008). Below-and aboveground *Spartina alterniflora* production in a Louisiana salt marsh. *Estuaries and Coasts*, *31*, 223–231.

Davi, H., Soudani, K., Deckx, T., Dufrene, E., Le Dantec, V., & Francois, C. (2006). Estimation of forest leaf area index from SPOT imagery using NDVI distribution over forest stands. *International Journal of Remote Sensing*, *27*, 885–902.

Davranche, A., Lefebvre, G., & Poulin, B. (2010). Wetland monitoring using classification trees and SPOT–5 seasonal time series. *Remote Sensing of Environment*, *114*, 552–562.

Decagon Devices (2008). *AccuPAR PAR/LAI ceptometer model LP–80: Operator's manual, version 1.2*. Decagon Devices, Pullman, WA.

Deegan, L. A., Hughes, J. E., & Rountree, R. A. (2002). Salt marsh ecosystem support of marine transient species. *Concepts and controversies in tidal marsh ecology* (pp. 333–365). Dordrecht, South Holland, The Netherlands: Springer Netherlands.

Delalieux, S., Somers, B., Hereijgers, S., Verstraeten, W. W., Keulemans, W., & Coppin, P. (2008). A near-infrared narrow-waveband ratio to determine Leaf Area Index in orchards. *Remote Sensing of Environment*, *112*, 3762–3772.

Evans, T. L., & Costa, M. (2013). Landcover classification of the Lower Nhecolândia subregion of the Brazilian Pantanal Wetlands using ALOS/PALSAR, RADARSAT–2 and ENVISAT/ASAR imagery. *Remote Sensing of Environment*, *128*, 118–137.

Filippi, A. M., & Jensen, J. R. (2006). Fuzzy learning vector quantization for hyperspectral coastal vegetation classification. *Remote Sensing of Environment*, *100*, 512–530.

Fitzgerald, D. M., Fenster, M. S., Argow, B. A., & Buynevich, I. V. (2008). Coastal impacts due to sea-level rise. *Annual Review of Earth and Planetary Sciences*, *36*, 601–647.

Friedl, M. A., McIver, D. K., Hodges, J. C., Zhang, X. Y., Muchoney, D., Strahler, A. H., Woodcock, C. E., Gopal, S., Schneider, A., Cooper, A., Baccini, A., Gao, F., & Schaaf, C. (2002). Global land cover mapping from MODIS: Algorithms and early results. *Remote Sensing of Environment*, *83*, 287–302.

Friess, D. A., Spencer, T., Smith, G. M., Möller, I., Brooks, S. M., & Thomson, A. G. (2012). Remote sensing of geomorphological and ecological change in response to saltmarsh managed realignment, the wash, UK. *International Journal of Applied Earth Observation and Geoinformation*, *18*, 57–68.

Gallagher, J. L., Reimold, R. J., Linthurst, R. A., & Pfeiffer, W. J. (1980). Aerial production, mortality, and mineral accumulation-export dynamics in *Spartina alterniflora* and *Juncus roemerianus* plant stands in a Georgia salt marsh. *Ecology*, *6*, 303–312.

Gamon, J. A., & Surfus, J. S. (1999). Assessing leaf pigment content and activity with a reflectometer. *New Phytologist*, *143*, 105–117.

Gilfillan, E. S., Page, D. S., Bass, A. E., Foster, J. C., Fickett, P. M., Ellis, W. G. H., Rusk, S., & Brown, C. (1989). Use of Na/K ratios in leaf tissues to determine effects of petroleum on salt exclusion in marine halophytes. *Marine Pollution Bulletin*, *20*, 272–276.

Gilmore, M. S., Civco, D. L., Wilson, E. H., Barrett, N., Prisloe, S., Hurd, J. D., & Chadwick, C. (2010). *Remote sensing and in situ measurements for delineation and assessment of coastal marshes and their constituent species, in: Remote sensing of coastal environment*. Boca Raton, Florida, USA: CRC Press, 261–280.

Gitelson, A., & Merzlyak, M. (1994). Quantitative estimation of chlorophyll-a using reflectance spectra: Experiments with autumn chestnut and maple leaves. *Journal of Photochemistry and Photobiology B: Biology*, *22*, 247–252.

Gitelson, A. A. (2004). Wide dynamic range vegetation index for remote quantification of crop biophysical characteristics. *Journal of Plant Physiology*, *161*(165–173), 2004.

Gitelson, A. A., Kaufman, Y. J., Stark, R., & Rundquist, D. (2002b). Novel algorithms for remote estimation of vegetation fraction. *Remote Sensing of Environment*, *80*, 76–87.

Gitelson, A. A., Keydan, G. P., & Merzlyak, M. N. (2006). Three-band model for noninvasive estimation of chlorophyll, carotenoids, and anthocyanin contents in higher plant leaves. *Geophysical Research Letters*, *33*, L11402.

Gitelson, A. A., Stark, R., Grits, U., Rundquist, D., Kaufman, Y., & Derry, D. (2002a). Vegetation and soil lines in visible spectral space: a concept and technique for remote estimation of vegetation fraction. *International Journal of Remote Sensing*, *23*, 2537–2562.

Gitelson, A. A., Vina, A., Ciganda, V., Rundquist, D. C., & Arkebauer, T. J. (2005). Remote estimation of canopy chlorophyll content in crops. *Geophysical Research Letters*, *32*.

Gitelson, A., Kaufman, Y., & Merzlyak, M. (1996c). Use of a green channel in remote sensing of global vegetation from EOS–MODIS. *Remote Sensing of Environment*, *58*, 289–298.

Gong, P., Pu, R., & Miller, J. R. (1995). Compact airborne spectrographic imager data. *Photogrammetric Engineering and Remote Sensing*, *61*, 1107–1117.

Goudie, A. (2013). Characterising the distribution and morphology of creeks and pans on salt marshes in England and Wales using Google Earth. *Estuarine, Coastal and Shelf Science*, *129*, 112–123.

Hansen, P. M., & Schjoerring, J. K. (2003). Reflectance measurement of canopy biomass and nitrogen status in wheat crops using normalized difference vegetation indices and partial least squares regression. *Remote Sensing of Environment*, *86*, 542–553.

Hardisky, M. A., Daiber, F. C., Roman, C. T., & Klemas, V. (1984). Remote sensing of biomass and annual net aerial primary productivity of a salt marsh. *Remote Sensing of Environment*, *16*, 91–106.

Hester, M. W., & Mendelssohn, I. A. (2000). Long-term recovery of a Louisiana brackish marsh plant community from oil–spill impact: vegetation response and mitigating effects of marsh surface elevation. *Marine Environmental Research*, *49*, 233–254.

Hinkle, R. L., & Mitsch, W. J. (2005). Salt marsh vegetation recovery at salt hay farm wetland restoration sites on Delaware Bay. *Ecological Engineering*, *25*, 240–251.

Hopkinson, C. S., Gosselink, J. G., & Parrando, R. T. (1978). Aboveground production of seven marsh plant species in coastal Louisiana. *Ecology*, *59*, 760–769.

Huete, A. R. (1988). A soil-adjusted vegetation index (SAVI). *Remote Sensing of Environment*, *25*, 295–309.

Huete, A., Didan, K., Miura, T., Rodriguez, E. P., Gao, X., & Ferreira, L. G. (2002). Overview of the radiometric and biophysical performance of the MODIS vegetation indices. *Remote Sensing of Environment*, *83*, 195–213 (2002).

Jackson, T. J., Schmugge, T. J., Parry, R., Kustas, W. P., Ritchie, J. C., Shutko, A. M., Bach, L. B., Haldin, A., Reutov, E., Novichikhin, E., B., Liberman, B., Shiue, J. C., Davis, M. R., Goodrich, D. C., Amer, S. B., & Bach, L. B. (1992). Multifrequency passive microwave observations of soil moisture in an arid rangeland environment. *International Journal of Remote Sensing*, *13*, 573–580.

Jensen, J. R. (1996). *Introductory digital image processing: a remote sensing perspective*. New York, New York, USA: Prentice–Hall Inc.

Jensen, J. R. (2007). *Remote sensing of the environment: An earth resource perspective*. New York, New York, USA: Prentice–Hall Inc.

Jensen, J. R., Rutchey, K., Koch, M. S., & Narumalani, S. (2002). Inland wetland change detection in the Everglades water conservation area 2A using a time series of normalized remotely sensed data. *Photogrammetric Engineering and Remote Sensing*, *61*, 199–209.

Jensen, R., Mausel, P., Dias, N., Gonser, R., Yang, C., Everitt, J., & Fletcher, R. (2007). Spectral analysis of coastal vegetation and land cover using AISA+ hyperspectral data. *Geocarto International*, *22*, 17–28.

Kearney, M. S., Stutzer, D., Turpie, K., & Stevenson, J. C. (2009). The effects of tidal inundation on the reflectance characteristics of coastal marsh vegetation. *Journal of Coastal Research*, *25*, 1177–1186.

Kennish, M. J. (2001). Coastal salt marsh systems in the US: A review of anthropogenic impacts. *Journal of Coastal Research*, *17*, 731–748.

Klemas, V. (2011). Remote sensing of wetlands: case studies comparing practical techniques. *Journal of Coastal Research*, *27*, 418–427.

Koch, E. W., Barbier, E. B., Silliman, B. R., Reed, D. J., Perillo, G. M., Hacker, S. D., Granek, E. F. , Primavera, J. H., Muthiga, N., Polasky, S., Halpern, B. S., Kennedy, C. J., Kappel, C. V., & Wolanski, E. (2009). Non-linearity in ecosystem services: temporal and spatial variability in coastal protection. *Frontiers in Ecology and the Environment*, *7*, 29–37.

Kovacs, J. M., King, J. M. L., de Santiago, F. F., & Flores-Verdugo, F. (2009). Evaluating the condition of a mangrove forest of the Mexican Pacific based on an estimated leaf area index mapping approach. *Environmental Monitoring and Assessment*, *157*, 137–149.

Kovacs, J. M., Wang, J., & Flores-Verdugo, F. (2005). Mapping mangrove leaf area index at the species level using IKONOS and LAI-2000 sensors for the Agua Brava Lagoon, Mexican Pacific. *Estuaries, Coastal and Shelf Science*, *62*, 377–384.

Laba, M., Downs, R., Smith, S., Welsh, S., Neider, C., White, S., Richmond, M., Philpot, W., & Baveye, P. (2008). Mapping invasive wetland plants in the Hudson River National Estuarine Research Reserve using Quickbird satellite imagery. *Remote Sensing of Environment*, *112*, 286–300.

Lefebvre, A., Corpetti, T., Bonnardot, V., Quénol, H., & Hubert-Moy, L. (2010). *Vineyard identification and characterization based on texture analysis in the Helderberg Basin (South Africa), 30th IEEE International Geoscience and Remote Sensing Symposium, 2852–2855 (Honolulu, Hawaii, 25–30 July 2010), 2010.*

Li–COR Inc. (2000). *LAI-2000 plant canopy analyzer: instruction manual*. Lincoln, Nebraska, USA: Li–COR, Inc.

Lillesand, T. M., Kiefer, R. W., & Chipman, J. W. (2008). *Remote sensing and image interpretation*. Hoboken, New Jersey, USA: John Wiley and Sons Ltd.

Lindstedt, D. M., & Swenson, E. M. (2006). *The case of the dying marsh grass, Louisiana Department of Natural Resources*. LA: Baton Rouge.

Lovelace, J. K., & McPherson, B. F. (1998). Restoration, creation, and recovery: Effects of Hurricane Andrew (1992) on Wetlands in Southern Florida and Louisiana. *National water summary on wetland resources. U. S. Geological Survey Water Supply Paper, 2425*, http://water.usgs.gov/nwsum/WSP2425/andrew.html.

Loveland, T. R., Zhiliang, Z., Ohlen, D. O., Brown, J. F., Reed, B. C., & Limin, Y. (1999). An analysis of the IGBP global land-cover characterization process. *Photogrammetric Engineering and Remote Sensing, 65*, 1021–1032.

Lyles, L. D., Namwamba, F., & Campus, B. R. (2005). Louisiana coastal zone erosion: 100+ years of landuse and land loss using GIS and remote sensing. *5th Annual ESRI Education User Conference, San Diego, California* (pp. 23–26) (July).

Markwell, J., Osterman, J. C., & Mitchell, J. L. (1995). Calibration of the Minolta SPAD-502 leaf chlorophyll meter. *Photosynthesis Research, 46*, 467–472.

Mishra, D. R., Cho, H. J., Ghosh, S., Fox, A., Downs, C., Merani, P. B. T., Kirui, P., Jackson, N., & Mishra, S. (2012). Post-spill state of the marsh: Remote estimation of the ecological impact of the Gulf of Mexico oil spill on Louisiana Salt Marshes. *Remote Sensing of Environment, 118*, 176–185.

Mishra, D. R., Ghosh, S., Hladik, C., O'Connell, J. L., & Cho, H. J. (2015). Wetland mapping methods and techniques using multi-sensor, multi-resolution remote sensing: successes and challenges. *Remote sensing handbook. vol. III*, . New York, New York, USA: Taylor and Francis (in press).

Mitsch, W. J., & Gosselink, J. G. (2007). *Wetlands.* Hoboken, New Jersey, USA: John Wiley and Sons.

Möller, I., Kudella, M., Rupprecht, F., Spencer, T., Paul, M., van Wesenbeeck, B. K., Wolters, G., Jensen, K., Bouma, T. J., Miranda-Lange, M., & Schimmels, S. (2014). Wave attenuation over coastal salt marshes under storm surge conditions. *Nature Geoscience, 7*, 727–731.

Morgan, P. A., Burdick, D. M., & Short, F. T. (2009). The functions and values of fringing salt marshes in northern New England, USA. *Estuaries and Coasts, 32*, 483–495.

Myneni, R. B., Keeling, C. D., Tucker, C. J., Asrar, G., & Nemani, R. R. (1997a). Increased plant growth in the northern high latitudes from 1981 to 1991. *Nature, 386*, 698–702.

Myneni, R. B., Nemani, R. R., & Running, S. W. (1997b). Estimation of global LAI and FPAR from radiative transfer models. *IEEE Transactions on Geoscience and Remote Sensing, 35*, 1380–1393.

Nackaerts, K., Coppin, P., Muys, B., & Hermy, M. (2000). Sampling methodology for LAI measurements with LAI-2000 in small forest stands. *Agricultural and Forest Meteorology, 101*, 247–250.

Nicholls, R. J., Hoozemans, F. M., & Marchand, M. (1999). Increasing flood risk and wetland losses due to global sea-level rise: regional and global analyses. *Global Environmental Change, 9*, S69–S87.

Pay, S. S., Das, G., Singh, J. P., & Panigrahy, S. (2006). Evaluation of hyperspectral indices for LAI estimation and discrimination of potato crop under different irrigation treatments. *International Journal of Remote Sensing, 27*, 5373–5387.

Pidgeon, E. (2009). Carbon sequestration by coastal marine habitats: Important missing sinks. *The management of natural coastal carbon sinks* (pp. 47–51). Gland, Switzerland: IUCN.

Pierce, L. L., Running, S. W., & Walker, J. (1994). Regional-scale relationships of leaf area index to specific leaf area and leaf nitrogen. *Ecological Applications, 4*, 313–321.

Pinar, A., & Curran, P. J. (1996). Grass chlorophyll and the reflectance red edge. *International Journal of Remote Sensing, 17*, 135–357.

Proisy, C., Couteron, P., & Fromard, F. (2007). Predicting and mapping mangrove biomass from canopy grain analysis using Fourier-based textural ordination of IKONOS images. *Remote Sensing of Environment, 109*, 379–392.

Ravens, T. M., Thomas, R. C., Roberts, K. A., & Santschi, P. H. (2009). Causes of salt marsh erosion in Galveston Bay, Texas. *Journal of Coastal Research, 25*, 265–272.

Rendong, L., & Jiyuan, L. (2004). Estimating wetland vegetation biomass in the Poyang Lake of central China from Landsat ETM data. *IEEE Transactions on Geoscience and Remote Sensing, 4*, 4590–4593.

Richardson, A. D., Braswell, B. H., Hollinger, D. Y., Jenkins, J. P., & Ollinger, S. V. (2009). Near-surface remote sensing of spatial and temporal variation in canopy phenology. *Ecological Applications, 19*, 1417–1428.

Richardson, A. D., Duigan, S. P., & Berlyn, G. P. (2002). An evaluation of noninvasive methods to estimate foliar chlorophyll content. *New Phytologist, 153*, 185–194.

Rosso, P. H., Ustin, S. L., & Hastings, A. (2005). Mapping marshland vegetation of San Francisco Bay, California, using hyperspectral data. *International Journal of Remote Sensing, 26*, 5169–5191.

Rouse, J. W., Haas, R. H., Jr., Schell, J. A., & Deering, D. W. (1974). Monitoring vegetation systems in the Great Plains with ERTS, third ERTS-1 symposium. *NASA Special Publication, NASA SP–351* (pp. 309–317).

Rundquist, D. C., Narumalani, S., & Narayanan, R. M. (2001). A review of wetlands remote sensing and defining new considerations. *Remote Sensing Reviews, 20*, 207–226.

Rundquist, D., Perk, R., Leavitt, B., Keydan, G., & Gitelson, A. (2004). Collecting spectral data over cropland vegetation using machine–positioning versus hand-positioning of the sensor. *Computers and Electronics in Agriculture, 43*, 173–178.

Schmidt, K. S., & Skidmore, A. K. (2003). Spectral discrimination of vegetation types in a coastal wetland. *Remote Sensing of Environment, 85*(8), 92–108.

Simard, M., Fatoyinbo, L. E., & Pinto, N. (2010). Mangrove canopy 3D structure and ecosystem productivity using active remote sensing. *Remote sensing of coastal environments* (pp. 61–78). Boca Raton, Florida, USA: CRC Press.

Stout, J. P. (1984). The ecology of irregularly flooded salt marshes of the northeastern Gulf of Mexico: A community profile. *Biological Report, 85*, Slidell, LA: U.S. Fish and Wildlife Service 97 pp.

Sugumaran, R., Meyer, J. C., & Davis, J. (2004). A web-based environmental decision support system (WEDSS) for environmental planning and watershed management. *Journal of Geographical Systems, 6*, 307–322.

Thenkabail, P. S., Smith, R. B., & De Pauw, E. (2000). Hyperspectral vegetation indices and their relationships with agricultural crop characteristics. *Remote Sensing of Environment, 71*, 158–182.

Tiner, R. W. (1996). Wetland definitions and classifications in the United States. *National water summary on wetland resources. US Geological Survey, water-supply paper, 2425.* (pp. 27–34).

Tiner, R. W. (2013). *Tidal wetlands primer: An introduction to their ecology, natural history, status, and conservation, the University of Massachusetts Press.* Massachusetts, USA: Amherst.

Turpie, K. (2013). Explaining the spectral red-edge features of inundated marsh vegetation. *Journal of Coastal Research, 29*, 1111–1117.

Vermote, E. F., Kotchenova, S. Y., & Ray, J. P. (2011). MODIS surface reflectance user's guide. MODIS land surface reflectance science computing facility, version, 1. (http://modis-sr.ltdri.org/guide/MOD09_Use rGuide_v1_3.pdf).

Wang, Y. (2010). *Remote sensing of coastal environments: an overview, in: Remote sensing of coastal ernvironments.* Boca Raton, Florida, USA: CRC Press, 1–24.

Wang, Y., Christiano, M., & Traber, M. (2010). Mapping salt marshes in Jamaica Bay and terrestrial vegetation in fire island national seashore using quickbird satellite data. *Remote sensing of coastal environments* (pp. 191–208). Boca Raton, Florida, USA: CRC Press.

Waple, A. (2005). *Hurricane Katrina.* NOAA, Asheville, NC: National Climatic Data Center.

Weis, J. S. (2010). Salt marsh. *Encyclopedia of Earth, environmental information coalition.* Washington, D.C: National Council for Science and the Environment.

White, M. A., Asner, G. P., Nemani, R. R., Privette, J. L., & Running, S. W. (2000). Measuring fractional cover and leaf area index in arid ecosystems: Digital camera, Radiation transmittance, and laser altimetry methods. *Remote Sensing of Environment, 74*, 45–57.

Zhang, C., & Xie, Z. (2012). Combining object–based texture measures with a neural network for vegetation mapping in the Everglades from hyperspectral imagery. *Remote Sensing of Environment, 124*, 310–320.

Zomer, R. J., Trabucco, A., & Ustin, S. L. (2009). Building spectral libraries for wetlands land cover classification and hyperspectral remote sensing. *Journal of Environmental Management, 90*, 2170–2177.